CHALMERS
UNIVERSITY OF TECHNOLOGY

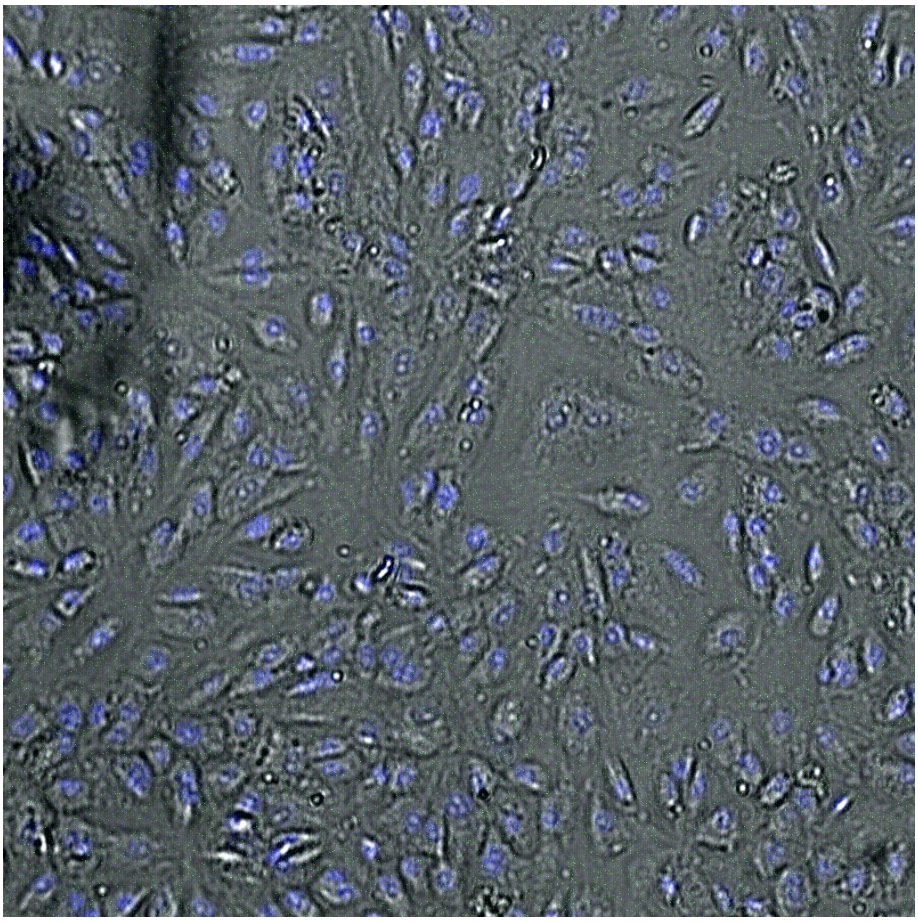

Vessel-on-a-Chip Development to Understand Systemically Administered Nanoparticles

Degree project report in Life Sciences

Fan Jia

DEPARTMENT OF LIFE SCIENCES
CHALMERS UNIVERSITY OF TECHNOLOGY
Gothenburg, Sweden 2024
www.chalmers.se

Degree project report 2024

Vessel-on-a-Chip Development to Understand Systemically Administered Nanoparticles

Fan Jia

CHALMERS
UNIVERSITY OF TECHNOLOGY

Department of Life Sciences
Chalmers University of Technology
Gothenburg, Sweden 2024

Vessel-on-a-Chip Development to Understand Systemically Administered Nanoparticles
Fan Jia

Supervisor: Elin Svensson, Department of LIFE Sciences
Examiner:Alexandra Stubelius, Department of LIFE Sciences

Degree project report 2024
Department of Life Sciences
Chalmers University of Technology
SE-412 96 Gothenburg
Sweden
Telephone +46 31 772 1000

Cover: Merged Vessel-on-a-chip confocal image illustrating the cell monolayer alignment.

Typeset in LaTeX
Gothenburg, Sweden 2024

Vessel-on-a-Chip Development to Understand Systemically Administered Nanoparticles

Fan Jia
Department of Life Sciences
Chalmers University of Technology

Abstract

Nanomedicine holds great promise for treating complex diseases, particularly due to its unique ability to sustain and target drug delivery. However, the validation method has been a great challenge to the development of nano-based therapeutics. The main reason is the unpredictable delivery dosage and lack of adequate preclinical trial methods that replicate the human biological environment for testing nanomedicine. This project introduced organ-on-a-chip (OOC) method to mimic the human vascular environment *in vitro* for studying the transportation of nanoparticles in human vessels. The goal was to use commercially available resources to increase the generalization and ease of adaptability for other labs working within the field of nanomedicine.

The build-up of this vessel-on-a-chip (VoC) was successfully achieved using a microfluidic chip from Ibidi along with a microfluidic set-up to stimulate the human umbilical vein endothelial cells (HUVEC) seeded in the chip. The cells formed an oriented endothelial cell (EC) monolayer mimicking the endothelium of a capillary under a 24-hour flow of 10dyn/cm^2. This monolayer acted as a barrier preventing NPs from extravasating into the tissue, which is an important aspect of nanoparticle delivery.

In addition, a computational fluidic dynamic (CFD) simulation approach was conducted to further enhance the predictability of NP transportation. The microfluidic simulation helped to explain unexpected phenomena during the flow experiment. Although the blood flow simulation had some limitations, it could provide useful insights when evaluating a potential uptake amount of NPs when administered systemically. This integrated study of combining VOC with CFD simulation enhances our understanding of NP behavior in human vessels but requires further optimization to be fully operational.

Keywords: VOC, Nanoparticle, laminar flow, HUVECs, CFD

Acknowledgements

I would like to express my deepest gratitude to my examiner, Docent Alexandra Stubelius, for her invaluable guidance and encouragement throughout this year-long project. This project could never been completed without Alex's support. I am also profoundly grateful to my supervisor, Elin Svensson, and everyone else in the group for their help and guidance in the lab.
Special thanks to my parents, my cat, and other family members for their emotional support. Meanwhile, I am also incredibly grateful to my friends Zhan, Isabella, Zhong, and all my other beloved friends who shared laughter, tears, happiness, and moments of despair. Their presence has been like thousands of sparkling lights illuminating my life path.

Fan Jia, Gothenburg, June 2024

List of Acronyms

Below is the list of acronyms that have been used throughout this thesis listed in alphabetical order:

NP	Nanoparticle
OoC	Organ-on-a-chip
VoC	Vessel-on-a-chip
CFD	Computational Fluid Dynamics
RBC	Red Blood Cell
DMSO	Dimethyl Sulfoxide
PPE	Personal Protective Equipment
HUVEC	Human Umbilical Vein Endothelial Cell
EC	Endothelial Cell
PC	Protein Corona
CAM	Cell Adhesion Molecule
SMC	Smooth Muscle Cell
PDMS	Poly(dimethylsiloxane)
Re	Reynolds number
COLI	Collagen type I
PDL	Poly-d-lysine
PLGA	Polylactic-co-glycolic acid
FITC	Fluorescein isothiocyanate
FBS	Fetal Bovine Serum
COP	Cyclo olefin polymer
COC	Cyclic olefin copolymer
TNS	Trypsin Neutralization Solution
Hepes BSS	Hepes Buffered Balancded Salt Solution
EDTA	Ethylenediamine tetraacetic acid
PLL	Poly-L-lysine
HPMEC	Human Pulmonary Microvascular Endothelial Cell

Nomenclature

Below is the nomenclature of parameters, and variables that have been used throughout this thesis.

Parameters

d	Diameter
b	Width of the channel
h	Height of the channel
π	Ratio of a circle's circumference to its diameter
Re	Reynolds number

Variables

Q	Flow rate
V	Flow velocity
μ	Dynamic Viscosity of the flow
τ	Shear Stress

Contents

List of Acronyms vi

Nomenclature vii

List of Figures x

List of Tables xii

1 Introduction 1
- 1.1 Background . . . 1
- 1.2 Purpose . . . 2
- 1.3 Goals . . . 2
- 1.4 Limitations . . . 2
- 1.5 Risk Assessment . . . 2
- 1.6 Ethical Aspect . . . 3

2 Theory 4
- 2.1 Challenges for Nanomedicine . . . 4
- 2.2 Vascular System . . . 5
  - 2.2.1 Function and Size . . . 5
  - 2.2.2 Capillary and Endothelium . . . 6
  - 2.2.3 Nanoparticle Extravasation over Endothelial Cells . . . 6
- 2.3 Hemodynamics . . . 7
  - 2.3.1 Blood Viscosity . . . 7
  - 2.3.2 Blood Flow Types and Velocity . . . 7
  - 2.3.3 Shear stress . . . 8
- 2.4 Vessel-on-a-chip . . . 9

3 Methods 10
- 3.1 Literature study . . . 10
- 3.2 Material . . . 10
- 3.3 VoC Optimization . . . 11
  - 3.3.1 Microfluidic chips . . . 11
  - 3.3.2 Cell culture and subculture . . . 12
  - 3.3.3 Microfluidic set-up optimization . . . 13
    - 3.3.3.1 Cell seeding in the microfluidic chip . . . 13
    - 3.3.3.2 Microfluidic set-up . . . 14

3.3.3.3 Flow rate set-up 14
3.3.4 Cell Alignment Confirmation 15
3.4 Measurement of NP extravasation over the endothelial layer 16
3.4.1 Confocal Fluorescence Microscope 16
3.4.2 Staining cells and nanoparticle treatment 17
3.4.3 Measurement and Image Processing 17
3.5 CFD Simulation of Flow and NP Behavior under Flow 17
3.5.1 Microfluidic Chip Simulation 17
3.5.2 Blood Flow Simulation 18
3.5.2.1 Models of Capillary and Arteriole 18
3.5.2.2 Flow and Particle Simulation 19

4 Results and Discussion **20**
4.1 Literature Study 20
4.2 VoC Optimization 20
4.2.1 Evaluation of Microfluidic Pump Setup for Long-Term Stability 20
4.2.2 Setup using BEOnChip 21
4.2.3 Setup using Ibidi Chips and Alignment Confirmation 23
4.3 NP Extravasation Evaluation over the Endothelial Monolayer 26
4.3.1 Under Static Condition 26
4.3.2 Under flow Condition 29
4.4 Simulation of Flow and NP Attachment 31
4.4.1 Microfluidic Chip Simulation 31
4.4.2 Blood Flow Simulation with RBCs and NPs 32

5 Conclusion **35**
5.1 Future initiative 35

A Appendix A **I**

List of Figures

2.1 Schematic image of the vascular system and the corresponding sizes of different parts. Image created in BioRender.com (2024) 5
2.2 Schematic image of the capillary structure which is formed by a single layer of endothelial cells. Image created in BioRender.com (2024) . . 6
2.3 Schematic image of the blood flow rates and types. Image created in BioRender.com (2024) 8

3.1 Pictures of all types of microfluidic chips utilized in the project. (A) Picture of BE-FLOW STANDARD chip. (B) Picture of BE-DOUBLEFLOW STANDARD chip. (C) Picture of Ibidi μ-Slide Ibitreat. (D) Picture of Ibidi μ-Slide Luer Glass Bottom chip. 11
3.2 Procedure schematic of cell seeding in the microfluidic chip. Image created in BioRender.com (2024) 13
3.3 Microfluidic system set up schematic. Image created in BioRender.com (2024) 14
3.4 Illustration of the Cell angle calculation. 16
3.5 Geometries of the BEOnChip (A) and Ibitreat (B) simulations. 18
3.6 Dimensions of a capillary (A) and an arteriole (B). 18

4.1 Photos of the optimized microfluidics set-up. (A) Optimized set-up with BEOnChip. (B) Cloudy cell medium was observed during the experiment. (C) Optimized set-up with Ibidi chip. (D) Thinned silicon tube was observed. 21
4.2 4X phase contrast microscopy images of channels of BEOnChips. (A) BE-FLOW chip before flow. (B) BE-FLOW chip after 5h flow. (C) BE-FLOW chip using mixed coating material after 2.5 hours at flow rate $200\mu l/min$. 23
4.3 EC alignment condition inside the Ibitreat chip. (A) 4X phase contrast microscopy images of ECs inside Ibitreat channel coated with COLI before flow. (B) 4X phase contrast microscopy images of ECs inside Ibitreat channel coated with COLI after 24-hour flow. (C) Cell detection and direction calculation before flow. (D) Cell detection and direction calculation after flow. (E) Cell direction histogram of figures (C) and (D). 25

4.4 4X phase contrast microscopy images of two special observations during the Ibidi chip fluidics experiment. (A) EC layer using Ibitreat chip coated with COLI before flow after 4-day flow. (B)ECs near the inlet of Ibitreat chip with PDL coating after 24-hour flow. 26
4.5 Images of NP transportation through EC layer under static condition. (A) Merged 20X confocal images of the monolayer at 10 min under static conditions. (B) Merged 20X confocal images of the monolayer after 3 hours in statics. (C) Flipped z-stack images. (D) The NP and nucleic fluorescence intensity plot at each z-stack. (E) The NP fluorescence intensity plot in different time points, the red area represents the inner cellular part. 28
4.6 Images of NP transportation through EC layer under flow condition. (A) Merged confocal images of the monolayer at 1 hour underflow. B Flipped image from the z-stack images at 1 hour. (C) The NP and nucleic fluorescence intensity plot at each z-stack layer. (D) The NP fluorescence intensity plot in different time points, the red area represents the inner cellular part. 30
4.7 Plots of flow simulation results of both BEOnChips and Ibitreat chip. (A) Velocity field flow rate plot of BEOnChip simulation. (B) Shear stress plot of BEOnChip simulation, and yz-slice plot of shear stress in the channel. (B)Velocity field flow rate plot of Ibitreat chip simulation. (D) Shear stress plot of Ibitreat simulation, and yz-slice plot of shear stress in the channel. 32
4.8 Plot of blood flow simulation and NP adhering result. (A) Red blood cells and nanoparticles traveling within the capillary flow model. (B) The surface of the capillary wall was modified to green to visualize particles adhering to the vessel wall. (C) Attachment of nanoparticles at different capillary shapes, highlighted in the circled areas. The left circle shows a curved capillary, while the middle depicts a straight capillary. (D) Red blood cells and nanoparticles traveling within the arteriole flow model. (E) Attachment of nanoparticles at arteriole wall. 33

List of Tables

3.1 **Dimension of four Microfluidics Chip** 12
3.2 **Endothelial Cell Density in Human Vessels and Corresponding Cell Concentration for Microfluidic Chip Experiments.** . 12
3.3 **Coating Time Requirements for Different Materials Across Various Microfluidic Chips** 14
3.4 **Flow Rate Set-up with corresponding Shear Stress and Time.** 15
3.5 **Staining compounds for nuclear and NPs, and their excitation wavelengths, emission wavelengths, and corresponding colors.** 16
3.6 **Flow and Particle Parameters used for Blood Flow Simulation and Particle Tracing.** 19

4.1 **Results of Flow Tests Using BEOnChips Under Different Setups** 22
4.2 **Results of Flow Tests Using Ibidi Chips Under Different Flow and Coating Setups.** 24
4.3 **Table of NP Attachment Results.** 34

1
Introduction

1.1 Background

Nanomedicine is the application of nanotechnologies to medicine [1], and since the success of nanoparticles (NP) used as carrier for the COVID-19 vaccine [2], the demand and potential of nanomedicine have significantly expanded. The translation and transportation of mRNA material inside the human body had been a challenge for genetic vaccines for years, where the delivery of mRNA in vivo kept meeting obstacles such as unstable and inefficient delivery [2]. The implementation of lipid nanoparticles as a cargo helped to targetly deliver of the mRNA citemrna. Other FDA approved nanomedicines include polymeric-based NPs such as Genexol-PM, treating more complex and recalcitrant diseases such as lung cancer [3],[4]. However, despite the success of these nano-drugs and the possibilities, nanomedicine still disadvantages the clinical translation of other FDA-approved drugs, potentiating their delivery, efficacy, and safety [5].

Based on a study from 2022, there were only 100 of 663 nanomedicines got approval on the market and the rest of 563 nanomedicines were in the clinical process or other stage [6], which indicates the challenge of clinical translation for NP-based medicine. One of the reasons that leads to clinical failure is low efficacy. NPs are mainly administered through injection which demands overcoming multiple biological processes such as circulation, accumulation, and cellular internalization. Such complicated biological procedures easily cause insufficient efficacy. FDA has yet to publish regulatory standards for nanomaterials, moreover, the gaps between human and animal models enhance the chance of clinical trial failure because of distinct interspecies differences.

This project is built upon a Vessel-on-a-Chip(VoC) model previously developed in the lab at Chalmers and is an extension of the work. Understanding how NPs are transported in the human body and untaken into cells are crucial problems, where particle chemical composition and properties such as size, charge, and shape has a huge influence on the interaction between the NPs and cellular environment [7]. The project is focused on a more thorough study of NP transportation within the vascular system, aiming to enhance the understanding and capabilities of NP design and application for drug delivery.

1.2 Purpose

The aim of this 30-hp thesis project is to establish a vessel-on-a-chip (VoC) model to enhance the understanding of polymeric NP transport within blood vessels to increase the success rate of clinically translated nanomedicine. The study of NP across the endothelial cell(EC) monolayers will be built on a microfluidic setup. The transportation of NP transportation inside the vascular system will also be studied using computational simulations.

1.3 Goals

This project encompassed multiple issues and scopes. Firstly, the wet lab experiment will begin with optimizing the microfluidics set-up to achieve a HUVEC monolayer in the chip channels. Based on that, the project involves the measurement of transit time and transport ratio of diverse NPs across HUVEC monolayers, both under statics and under flow conditions. The dry lab of the project entails computational fluid dynamics (CFD) simulation within the microchip, incorporating different blood flow scenarios of NP dispersions within the vascular environment.

1.4 Limitations

The project exclusively uses HUVEC cells, indicating that the findings may not be directly applicable to other cell lines. Given the differential of the particle properties, the results are specific to the NPs tested in this study, focusing on how these properties affect transportation efficiency. The VoC is a module that mimics the biological environment of a human vessel and, thus can not completely represent the response of the human body. Additionally, due to the lack of incubation setup within the microscope, the measurement of the NP through VoC would only be conducted at specific time points. In the simulation part, the Turbulent Flow module was not feasible due to the requirement of a computer with a better processing unit, and the particle shape defaulted to be spherical, thus physical replication of the red blood cell (RBC) shape was limited.

1.5 Risk Assessment

The materials used in this project, Dimethyl Sulfoxide (DMSO) and Fetal Bovine Serum (FBS), both have a moderate hazard level.

- DMSO was utilized as a cryoprotectant for cells, DMSO can cause skin and respiratory irritation and be absorbed through the skin, leading to potential systemic effects. It is also combustible under certain conditions.

- FBS was used during the measurement of nanoparticle transmission. FBS carries a low but present risk of biological contamination and can potentially cause allergic reactions in some individuals.

To avoid these risks, both substances were handled with appropriate personal protective equipment (PPE) including lab coats and gloves. All preparations were conducted under a laminar flow hood to minimize the risk of direct contact with skin and eyes, and to avoid inhalation.

1.6 Ethical Aspect

The success of developing such an NP testing module has the potential to replace animal testing that is still frequently demanded for developing new drugs such as in nanomedicine [6], [8]. From an ethical perspective, the replacement of animal testing is worth to investigate. Animal models do not fully represent the human response, which is particularly important in nanomedicine, where nano-delivery systems are designed to target specific cells or tissues in the human body. This indicates that a working protocol based on VoC for NP delivery could not only reduce the reliance on animal test but also speed up the procedure of translating nanomedicines into clinical trials. The VoC approach aligns with ethical principles by minimizing animal suffering and improving the accuracy and efficiency of preclinical testing.

2

Theory

2.1 Challenges for Nanomedicine

NPs utilized in the nanomedicine field vary in size, shape, material compositions, and surface charge [9].NP sizes range usually from 1 to 500 nm [1] and include various materials such as lipid-based nanomedicines, polymer-based nanomedicines, nanocrystals, inorganic nanoparticles, and protein-based nanomedicines [3],[9]. Due to such diversity, NP has the capacity to deliver bioactive molecules to target locations inside the human body, including therapeutic agents and imaging contrast enhancers in medical applications [1]. Polymeric-based NP, in particular, are excellent vehicles for controlled drug release due to their stability and biocompatibility [10]. Nanomedicine has been proven to reduce side effects and increase the efficacy of existing medicines for chronic inflammation, and NP could facilitate the transport of unstable and toxic substances [1].

Despite the broad application possibility of NP, disadvantages of NP include cytotoxicity and incorrect dosage [11]. In an analysis of NP delivery to tumor in both clinical and preclinical stages, the improperly designed injection routine and dosage resulted in a median of only 0.7% of the administered nano-based medicine accumulating in the target tissue after injection [12]. When the NPs enter the blood circulation, they are distributed throughout the body into non-targeted organs, particularly into the liver, which functions as a biological filter in the human body. Up to 45% of administered 500 nm polymeric NPs can accumulate in the liver, where they are then degraded, thus increasing the hepatic burden and potential toxicity [11],[13].

Another important phenomenon that occurs after NP enters the blood circulation is the protein corona (PC) effect, caused by proteins binding and coating the NP surface [14].The PC could affect the size change and surface properties of the NP, thereby influencing the delivery efficiency and uptake into the target tissue. Although the PC is hard to avoid during nanomedicine design, some formulations of polymer-based NP have successfully limited the interaction between NP and plasma proteins [14],[15]. For instance, an NP was synthesized with different hydrophilic polymers by Alberg's et al, resulting in significantly fewer plasma proteins on the NPs' surfaces [15].

2.2 Vascular System

2.2.1 Function and Size

The delivery of therapeutics to the target tissue mainly relies on the network of blood vessels within the body [16]. As Figure 2.1 shows, the blood circulation consists of three parts, each with characterized functions and different sizes. First, arteries and arterioles convey blood from the heart to the capillary network, where the red blood cells carry oxygen and other nutrients. Then the capillaries deliver blood with nutrients to tissues and the blood from the tissue is collected by larger veins and venules, completing the circuit of circulation [17]. Capillaries typically have a diameter range of 8 to 10 μm, while the major vessels like the aorta and the vena cava have diameters of about 30,000 μm [17],[18].

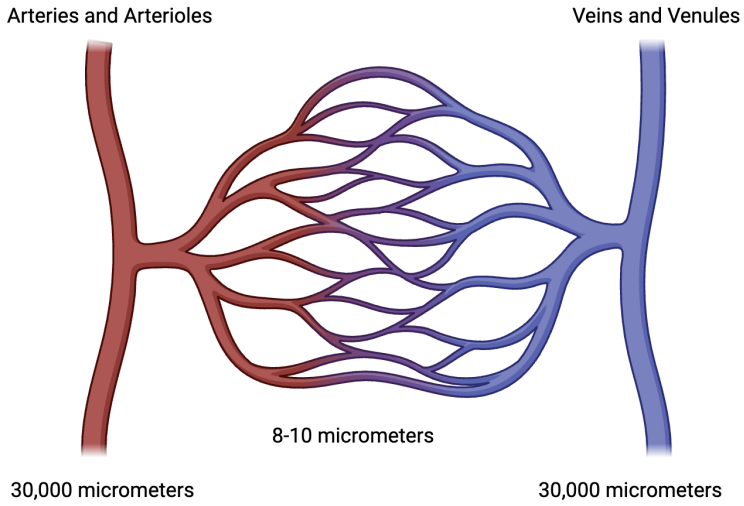

Figure 2.1: Schematic image of the vascular system and the corresponding sizes of different parts. Image created in BioRender.com (2024)

2.2.2 Capillary and Endothelium

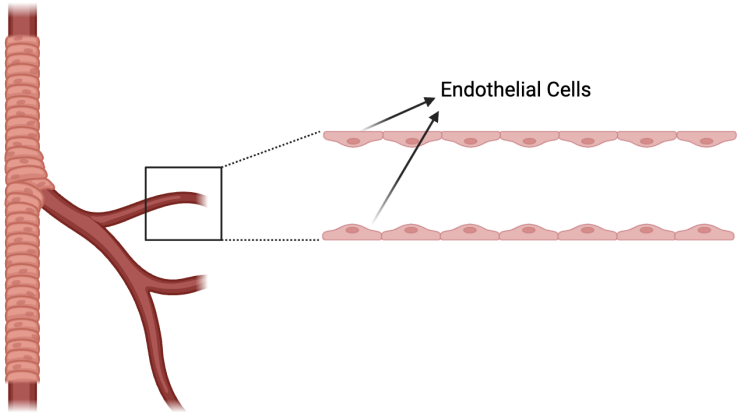

Figure 2.2: Schematic image of the capillary structure which is formed by a single layer of endothelial cells. Image created in BioRender.com (2024)

Unlike a large artery that is covered and supported by ECs and smooth muscle cells (SMC), the capillary vessel wall is a tube-like structure consisting of only endothelium, a single monolayer of ECs as shown in Figure 2.2. ECs across the vascular tube are thin and oriented cells that are roughly 50–70 μm long, 10–30 μm wide, and 0.1–10 μm thick [19]. Approximately 10 to 60 $\cdot 10^{12}$ ECs in the human body form about 300-1000 m^2 endothelium surface. ECs are laterally opposed to each other with a 10-20 nm gap between neighboring cell membranes [17].

The endothelium forms the inner cellular lining of all blood vessels and the alignment of ECs is flow-dependent [20]. The capillary vessel wall is a tube-like structure consisting of the endothelium, a single monolayer of ECs that separate the bloodstream from other tissues. Individual ECs are rounded and randomly oriented under static conditions [21], while ECs across the vascular cube are thin and oriented cells with a rectangular-like shape [19]. Long axes are oriented in the direction of blood flow, although ECs of the pulmonary are shorter and wider than aortic ECs [20].

2.2.3 Nanoparticle Extravasation over Endothelial Cells

The endothelium is a semi-permeable barrier that is modified in response to specific stimuli [22]. Transportation across the endothelium can consist of transcellular pathways, where the substance is transmitted through the EC, or paracellular pathways, where the substance is transmitted through the inter-endothelial junctions [23]. Transcellular transport consists of passive transport, passive diffusion, active transport, or endocytosis [24]. The internalization process of nanocarriers via cell adhesion molecule (CAM)-mediated endocytosis typically occurs within 15 to 20 minutes, indicating a relatively efficient uptake mechanism [16].

2.3 Hemodynamics

Hemodynamics is the study of blood flow distribution and blood pressure in the vascular system [25]. The special cytoskeletal components, stress fibers, inside ECs can detect the shear forces of blood flow and react by modifying their cytoskeletal structure [26]. This adjustment subsequently changes the tension exerted on junction proteins, indicating the formation of endothelial layer [27],[28]. The key factor affecting the formation and maintenance of the endothelial layer in response to the blood flow are the blood viscosity, the flow types and rate, and the shear stress [29],[30].

2.3.1 Blood Viscosity

Blood is a Non-Newtonian fluid and the viscosity(μ) of the blood varies in the vascular system, it is generally modeled as a Newtonian fluid in computational hemodynamics studies [31]. The viscosity varies mainly related to the RBCs and plasma factors [32]. Plasma is a Newtonian fluid with a non-changeable viscosity value of around 1.2–1.3 cP at $37°C$. The Fåhræus-Lindqvist is a plasma-skimming behavior of blood flow in smaller capillaries with a diameter under 0.3mm, while RBCs only distribute in the center of the vessel, leaving plasma near the vessel wall [33]. This effect leads to the viscosity value of adult healthy blood at around 4 cP at $37°C$ reducing to around 2 cP in small capillaries [32], [34]. Contributing to this change also stems from RBC having different formations and shapes in the vascular system. In a capillary with a diameter of approximately 5 μm, RBCs must deform to pass through this narrow passage, leading to a lower viscosity. In contrast, RBC tends to be more aggregating at larger vessels, causing the increasing of viscosity.

2.3.2 Blood Flow Types and Velocity

Blood flow is defined as the amount of blood flowing through the lumen of a blood vessel at a given time. Blood flow varies at different vascular parts as Figure 2.3 shows, although laminar flow is the most common flow of blood[18].

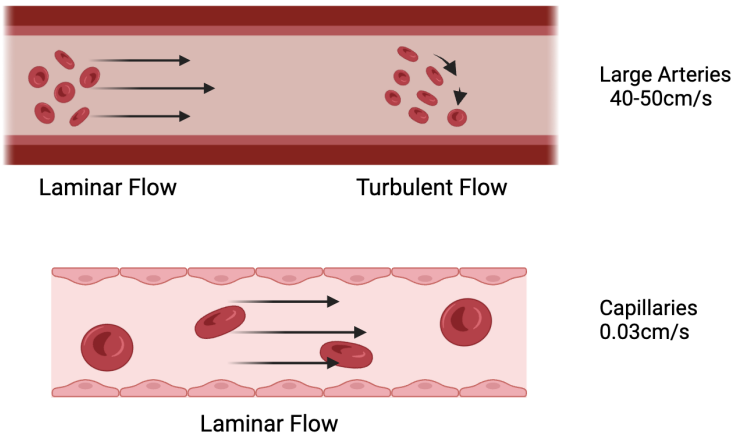

Figure 2.3: Schematic image of the blood flow rates and types. Image created in BioRender.com (2024)

In bigger arteries, the flow velocity can reach 40-50 cm/s, resulting in turbulent flow due to the high-speed flow conditions. Meanwhile, the blood velocity is around 0.03cm/s in the smallest capillaries, resulting in a laminar flow. The volume flow rate Q can be calculated by the equation below, where V represents the flow velocity and d represents the diameter of the vessels.

$$Q = V \cdot \pi d^2/4 \tag{2.1}$$

The physical nature of a flow field may be characterized by the Reynolds number (Re) [35]. When the Re value reaches above 4000, the flow can be considered turbulent, when the laminar has a Re value lower than 2000. Re value of flow in a pipe is calculated as follows:

$$Re = V d\rho/\mu \tag{2.2}$$

where V represents the velocity, d is the diameter of the pipe, ρ is the density of the flow and μ is the dynamic viscosity of the flow.

2.3.3 Shear stress

Shear stress (τ) is the tangential force of the flow onto the flow container surface and is essential for proper EC function [36]. ECs under directed exposure to the blood flow force mechanically responds to the signal and aligns with the blood streamline [37]. Shear stress in vessels is calculated as:

$$\tau_{vessel} = \frac{32 \cdot \mu Q}{\pi d^3} \tag{2.3}$$

where μ represents the viscosity, Q represents the flow rate, d is the diameter of the vessel, and π the ratio of the circumference of a circle to its diameter.
Shear stress in a parallel plate chamber is calculated in a similar way:

$$\tau_{chamber} = \frac{6 \cdot \mu Q}{bh^2} \tag{2.4}$$

where b and h represent the width and height respectively.

The endothelium is exposed to high-level shear stress up to 70 dyn/cm^2 in arteries and to 1 dyn/cm^2 in veins, while in capillaries the range of shear stress is 10 to 20 dyn/cm^2 [37].

2.4 Vessel-on-a-chip

VoC is a type of OoC and an in vitro cell culture technique that builds up microfabricated vessels to mimic blood vessels. It is particularly integrated for studying of transvascular transport and cell-tissue interactions [38]. To construct a VoC, vascular cells, such as ECs and SMCs, as well as microfluidic devices including a flow setup and microfluidic chip are required. Common method for building VoC involves seeding ECs into a microchannel-based chip and connecting the chip to the microfluidic flow system. The most frequently used material of the chip is poly(dimethylsiloxane) (PDMS).

Many NP studies employ VoC or other OoC technology involving ECs [39], [40]. Namdee's project utilized VoC to evaluate the imagination of nano- and microsphere in microvessels by changing the hemodynamic conditions, such as the size of the microfluidic chip and the flow speed [41]. He suggested that the microspheres outperformed nanospheres in adhering to the microvessel wall. Another example of OoC application is Kwak's study of NP transportation around a simulated tumor [42]. In the project, a tumor-on-a-chip platform was established, combining blood vessels, tumor tissue, and lymph vessels through three different types of microchannels in the same microfluidic chips. This model was developed to investigate which properties of NPs affect targeted NP delivery in cancer therapy. The study showed that NP with smaller diameters could diffuse through the tumor more efficiently.

3
Methods

This project involves literature studies, experimental research, and computational simulations. The experiment in the laboratory generally consisted of two parts, first establishing the VoC, and then conducting measurement of NPs behavior and uptake in the VoC.

3.1 Literature study

In this project, a wide range of literature studies were needed to support the research. The sources utilized included databases such as PubMed, COMSOL gallery, and Reaserchgate. Since the project consists of experiments with microfluidics chips in the laboratory as well as simulations, the procedure of cell subculture and microchip adherence process was studied. The protocol and tutorials from the chip company and the simulation software were also referenced.

3.2 Material

The materials and equipment used in the study included HUVECs, the HUVEC cell medium, and DetachKit from PromoCell (Heidelberg, Germany), FBS was used during NP transportation experiments. Coating materials included Collagen type I (COLI), sourced from rat tails with a concentration of 4.24 mg/mL (Corning, New York, USA) and poly-D-lysine (PDL) hydrobromide (Merck, Darmstadt, Germany). The study also utilized BE microfluidic chips, specifically the BE-FLOW STANDARD chip and BE-DOUBLEFLOW STANDARD chip, both from BEOnChip (BEOnChip S.L. Zaragoza, Spain), as well as Ibidi μ-Slide I Luer Glass Bottom chips and Ibitreat chips from Ibidi (Ibidi, Gräfelfing Germany).
Additionally, 190 nm poly(lactic-co-glycolic acid) (PLGA) nanoparticles with fluorescein isothiocyanate (FITC) labeling were used. The study employed phase and confocal microscopes (Nikon, Japan), Nuclear Stain (Hoechst 33342), and microfluidic equipment including a peristaltic pump (Fischer Scientific, Massachusetts, USA), a connecting kit(Ibidi, Gräfelfing Germany), Silicone Tubing (Darwin Microfluidics, Paris, France) and Falcon Tube (Darwin Microfluidics, Paris, France).

3.3 VoC Optimization

3.3.1 Microfluidic chips

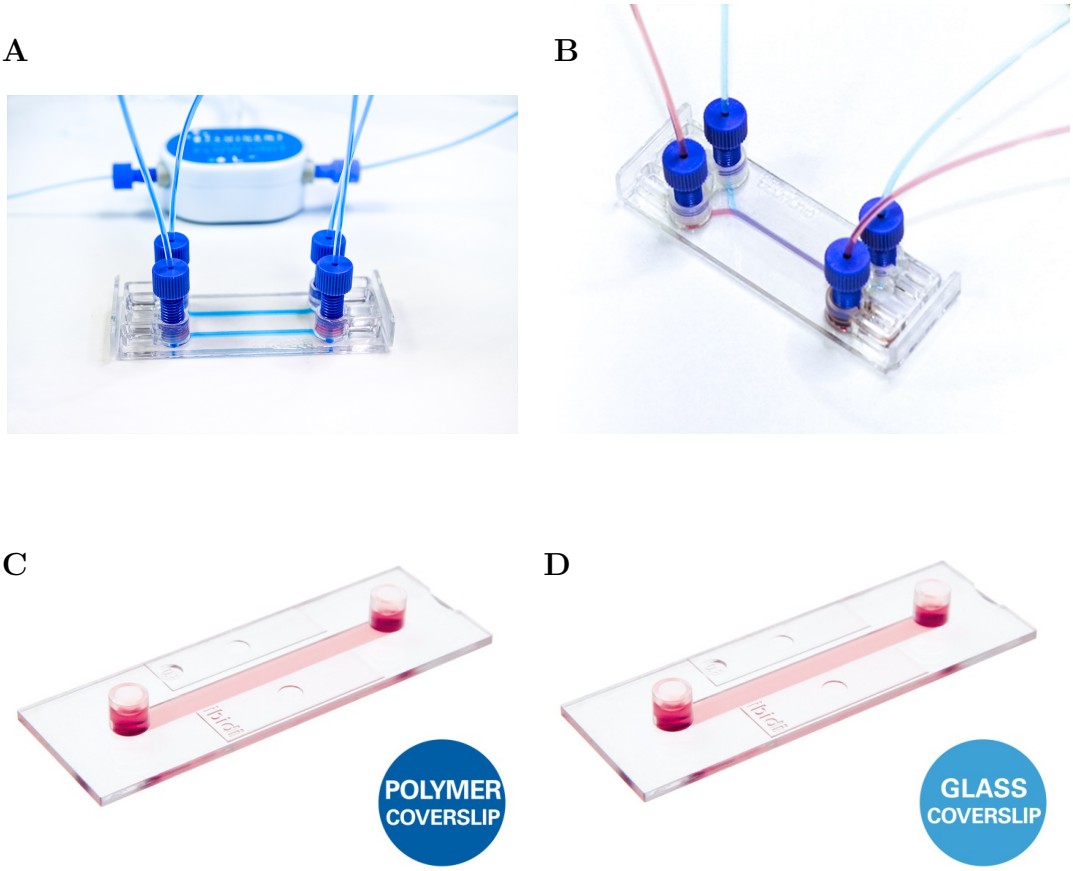

Figure 3.1: Pictures of all types of microfluidic chips utilized in the project. (A) Picture of BE-FLOW STANDARD chip. (B) Picture of BE-DOUBLEFLOW STANDARD chip. (C) Picture of Ibidi μ-Slide Ibitreat. (D) Picture of Ibidi μ-Slide Luer Glass Bottom chip.

Four types of microfluidic chips from two brands were utilized in the project, BE-flow STANDARD in Figure 3.1A (BEOnChip S.L. Zaragoza, Spain), BE-doubleflow STANDARD in Figure 3.1B (BEOnChip S.L. Zaragoza, Spain), μ-Slide I Luer 0.4 mm IbiTreat in Figure 3.1C (Ibidi, Gräfelfing Germany) and μ-Slide I Luer 0.4 mm glass bottom in Figure 3.1D (Ibidi, Gräfelfing Germany). The two BE chips are made from Cyclo olefin polymer (COP) and cyclic olefin copolymer (COC), which claim to be medical-grade plastics, and had two narrow channels of the same size. The Ibidi ibitreat μ-Slide chip (Ibitreat) has a modified surface with good surface adhesion and hydrophilicity, while the Ibidi μ-Slide glass bottom chip (IbGlass) has a glass surface. The dimensions of the channels in the chips are listed in Table 3.1

below.

Table 3.1: Dimension of four Microfluidics Chip

Microfluidic Chip Parameters			
Chip Type	**Width (mm)**	**Height (μm)**	**Length (mm)**
BEOnChip (Both)	1.5	375	4.5
Ibitreat	1.5	400	5
IbiGlass	1.5	450	5

3.3.2 Cell culture and subculture

In this project, HUVECs were used according to protocol from PromoCell. The cells were stored in the $-150°C$ freezer and then thawed in a $37°C$ water bath. The thawed cells were transferred into a T75-flask filled with 10 ml HUVEC cell medium and cultivated at $37°C$, 5% CO_2 incubator, and were subcultured when reached a confluency of 70-90%. DetachKit was used during subcultivation to detach the cells. Briefly, the cells were washed with Hepes Buffered Balanced Salt Solution (BSS) for 15 seconds and the Trypsin/ethylenediamine tetraacetic acid (EDTA) solution was used to detach the cells from the flask surface. After 5 minutes, the Trypsin Neutralization Solution (TNS) was added to neutralize the trypsin. The cell suspension was transferred into a falcon tube for centrifugation at 500xg for 5min. Meanwhile, the detached cells were counted by Cell Counters (Thermo Fisher, USA) to determine the total amount of the ECs in the tube. After centrifugation, the supernatant was removed and HUVEC cell medium was added to resuspend the cells at the desired concentration of either $2.5 \times 10^6 cells/ml$ or $3 \times 10^6 cells/ml$ depending on the chip type, as seen in Table 3.2.

Table 3.2: Endothelial Cell Density in Human Vessels and Corresponding Cell Concentration for Microfluidic Chip Experiments.

Endothelial Cell Density and Concentration	
Condition	**Cell Density/Concentration**
Human Vessel EC Density	$0.7 - 3.2 \times 10^5$ cells/cm^2
In Vitro EC Density on Chip	1×10^5 cells/cm^2
Cell Concentration for Ibidi Chip	2.5×10^6 cells/ml
Cell Concentration for BEOnChip	3×10^6 cells/ml

3.3.3 Microfluidic set-up optimization

3.3.3.1 Cell seeding in the microfluidic chip

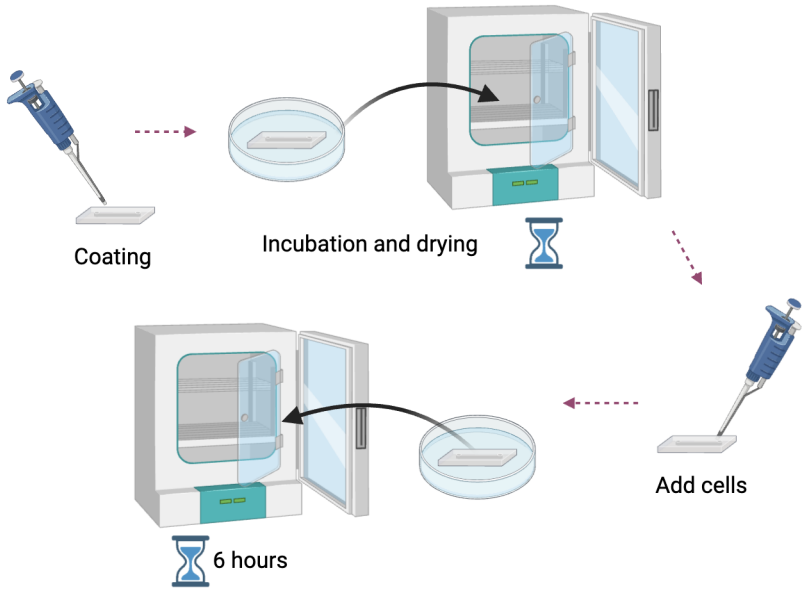

Figure 3.2: Procedure schematic of cell seeding in the microfluidic chip. Image created in BioRender.com (2024)

The cell seeding routine for all four chips was similar, as illustrated in Figure 3.2. The process started by coating the channels inside the chip with either COLI or PDL at the corresponding concentration and volume, as detailed in Table 3.3. The coated chips were put inside a Petri dish and incubated for the required time by the coating solution. After incubation, the coated surfaces were thoroughly washed with Dulbecco's Phosphate Buffered Saline (DPBS) 2-3 times. The cell suspension, prepared at the desired cell concentration, was then introduced into the channels. For the HUVECs to form a confluent layer, the chip seeded with cells was placed into the Petri dish and incubated for at least 6 hours.

Table 3.3: Coating Time Requirements for Different Materials Across Various Microfluidic Chips

Coating Parameters for Various Microfluidic Chips					
Chip Type	**Channel Volume**	**Coating Material**	**Coating Concentration**	**Incubation Time**	**Drying Time**
Ibitreat	100 μl	COLI	250 $\mu g/ml$	30 min	-
	100 μl	PDL	250 $\mu g/ml$	5 min	>16 h
IbGlass	125 μl	COLI	250 $\mu g/ml$	30 min	-
	125 μl	PDL	250 $\mu g/ml$	5 min	>16 h
Beflow/BeDF	28.5 μl	COLI	300 $\mu g/ml$	30 min	-
	28.5 μl	PDL	200 $\mu g/ml$	5 min	>16 h

3.3.3.2 Microfluidic set-up

To avoid contamination and improve the fluidic procedure, a connecting kit and a Microfluidic Reservoir of a 50 mL Falcon Tube were connected to the pump and the chip was changed. A peristaltic pump and 2 mm 3-stop Platinum-cured Silicone Tubing were used in this set-up as Figure 3.3.

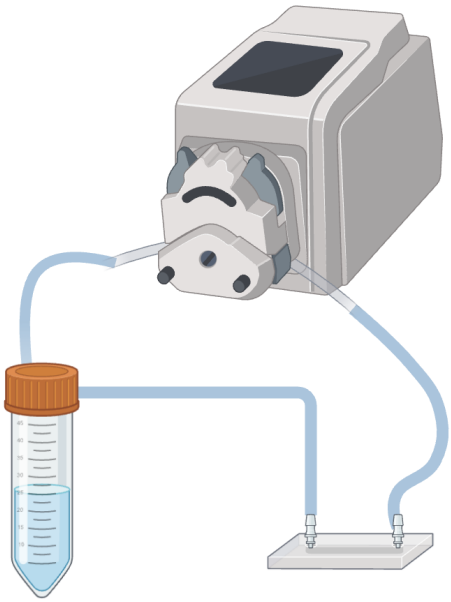

Figure 3.3: Microfluidic system set up schematic. Image created in BioRender.com (2024)

3.3.3.3 Flow rate set-up

The viscosity of HUVEC cell media is 0.8 cP. Based on the dimension in Table 3.1 and equations 2.1, 2.2 and 2.4, the relation between flow rate V in unit ml/min and

shear stress τ in unit dyn/cm^2 could be simplified as:

$$\tau_{beon} = 3.79V \tag{3.1}$$

$$\tau_{ibitreat} = V \tag{3.2}$$

$$\tau_{ibGlass} = 0.79V \tag{3.3}$$

The channel dimensions for both BEOnChip were the same, thus the corresponding calculations were conducted accordingly. The designed flow parameters and time span for the flow experiment were calculated using the equations above in Table 3.4. The flow rate was designed to increase gradually until it reached the shear stress level at 10 dyn/cm^2 to reduce the risk of cell detachment.

Table 3.4: Flow Rate Set-up with corresponding Shear Stress and Time.

Microfluics Flow Set-up Parameters			
Chip type	**Flow Rate** ml/min	**Shear Stress** dyn/cm^2	**Time Span**
Both BEOnChips	0.5	2	30min
	1.3	5	30min
	2.6	10	infinite
Ibitreat	2	2	30 min
	5	5	30 min
	10	10	infinite
IbiGlass	2.5	2	30 min
	6.3	5	30 min
	12.7	10 m	infinite

3.3.4 Cell Alignment Confirmation

A MATLAB function was developed to evaluate the alignment of the ECs with the flow direction. The function comprised of two parts, cell detection, and cell direction evaluation. In the detection part, the main Matlab functions used were **adapthisteq** to enhance the contrast, while **imclose** and **edge** were employed for finding the cell boundaries. The flow direction was considered to be 0 degrees as Figure 3.4 shows. The angle difference between the cells and the flow direction was determined by drawing the longest quiver within the cell boundary and calculating the coordinates of its endpoints. This approach provided an accurate evaluation of cell orientation related to the flow.

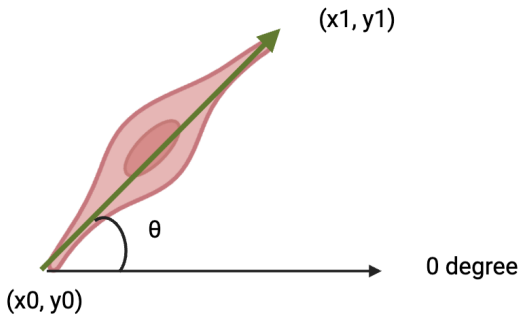

Figure 3.4: Illustration of the Cell angle calculation.

3.4 Measurement of NP extravasation over the endothelial layer

Fluorescent molecules were used for labeling the cells and the NP during imaging. The EC nuclei was stained by the fluorescent dye Hoechst 33342, and the 190nm polylactic-co-glycolic acid (PLGA) NPs were loaded with FITC (Table 3.5).

Table 3.5: Staining compounds for nuclear and NPs, and their excitation wavelengths, emission wavelengths, and corresponding colors.

Fluorescent Staining for Nuclear and Nanoparticles				
	Fluorescent Dye	**Excitation Wavelength**	**Emission Wavelength**	**Color**
Nuclear	Hoechst 33342	346nm	460nm	Blue
NP	FITC	495nm	519nm	Green

3.4.1 Confocal Fluorescence Microscope

The measurement was conducted with a Confocal Fluorescence Microscope, a commonly used tool for high-resolution bioimaging. The sample, stained with a fluorescent label, was scanned with a corresponding laser, and the emitted light from the label was then captured by the microscope's detector. The signal was then processed into image form, and several images along the z-axis were combined to form a Z-stack. The Z-stack images allow for a detailed 3-dimensional study of the sample. The working principle of the z-stack could be simplified as:

1. Laser scanning of the first in-focus layer along the z-axis.
2. The objective lens and the corresponding focal plane move down with one step size, and the second layer of the sample is captured by repeating the laser scanning.
3. Finally, the layers are sequentially packed as a Z-stack image.

3.4.2 Staining cells and nanoparticle treatment

After confirming the alignment of the EC monolayer, a $10\mu g/ml$ Hochest 33342 suspension was added into the channel followed by a 30-minute incubation. The channel was then washed with cell medium before adding the prepared suspension of labeled NPs. For static conditions, a 150 µl of HUVEC cell medium of NP concentration of $20\mu g/ml$ was incubated for 30 minutes before being added into the channel. For flow conditions, 500 µl of FBS was incubated with an NP concentration of $15\mu g/ml$ for 30 minutes. The FBS suspension, along with 4.5 ml of cell medium resulting in a final NP concentration of $1.5\mu g/ml$, was then added to a Falcon tube under the microfluidic conditions.

3.4.3 Measurement and Image Processing

Based on the given excitation laser, three color channels of every layer of the sample were captured: the blue channel collected the Hoechest fluorescence signal, the green channel collected the FITC fluorescence, and the transmitted non-fluorescent channel revealed the morphology of the cells. The images were scheduled to be taken at 10 minutes, 30 minutes, 1 hour, 2 hours, and 3 hours after introduction of the NPs into the chip. The step size of layer shifting was set as 1 or 2 μm.
Two different fluorescence signal intensities at each z-stack layer were then calculated. The position of the ECs monolayer on the z-axis was determined by the highest blue intensity z-coordinate in each stacked image. NP fluorescence intensity over time was then correlated and plotted.

3.5 CFD Simulation of Flow and NP Behavior under Flow

COMSOL Multiphysics is a widely used simulation software that supports various modules for different types of studies. In this project, the Laminar Flow study and the Particle Tracing for Fluid Flow study submodules were utilized, based on the guidelines provided in the COMSOL user guide[43],[43]. The simulation consisted of three parts, the shear stress and flow velocity simulation of different chips used in the project were simulated with a Laminar Flow module, and the blood flow simulation with RBCs and NPs in an artery and a capillary was studied with Laminar Flow and Particle Tracing modules. The related equations used for different modules are included in Appendix A.

3.5.1 Microfluidic Chip Simulation

The laminar flow mode was used since the Re values for all the chips were around 50 calculated with the equation 2.1. The geometries of the chips were built according to the chip features and the dimension Table 3.1. Since the dimensions of both Ibidi chips were similar and the dimensions of the BEOnChips were the same, only one

of each model was built in this project. Figures 3.5A and 3.5B below illustrate the geometries of the chip channel.

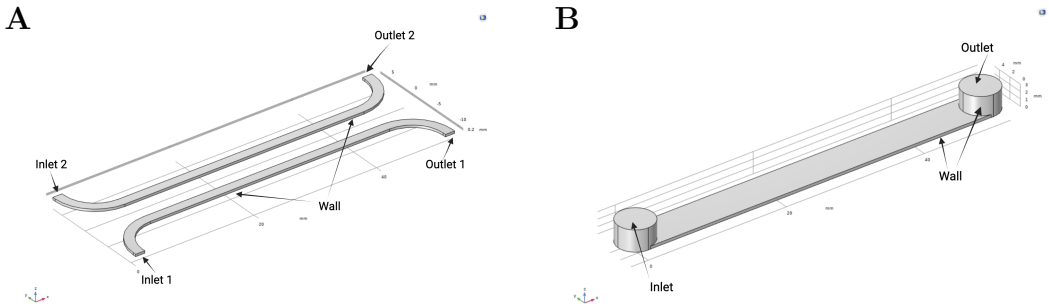

Figure 3.5: Geometries of the BEOnChip (A) and Ibitreat (B) simulations.

The inlet and outlet represent the location where the fluid enters and leaves the channel. The wall boundary was set as the no-slip condition. The inlet flow properties were set as the same as in VoC experiments, the flow rate for BEOnChip was defined as 3 ml/min and 10 ml/min for Ibitreat chip to match the microfluidics set-up.

3.5.2 Blood Flow Simulation

3.5.2.1 Models of Capillary and Arteriole

As Figure 3.6A shows, a partial capillary model was established, and the diameters of the capillaries varied from 8 to 10 μm. The arteriole was modulated as a tube of 5 mm diameter to match the width of the Ibidi chip in Figure 3.6B.

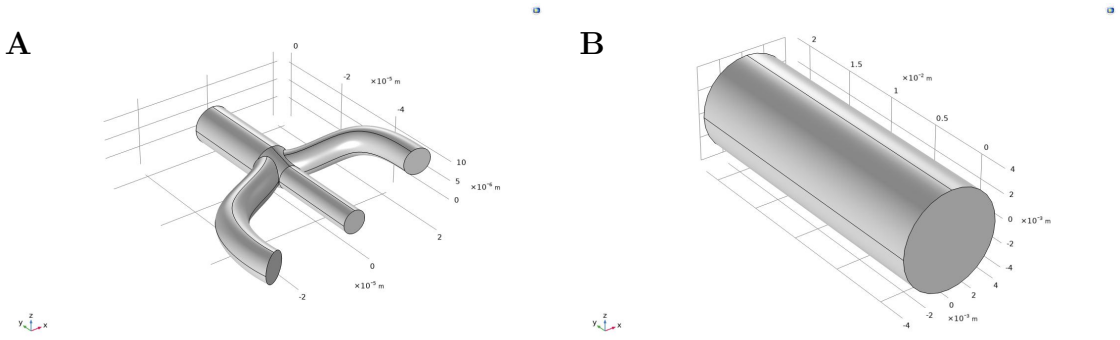

Figure 3.6: Dimensions of a capillary (A) and an arteriole (B).

3.5.2.2 Flow and Particle Simulation

Laminar flow and particle tracing studies were performed for both simulations. The wall condition was set to 'stick' to mimic particle attachment to the vessel wall. Two sizes of NP were studied for capillary flow simulation, whereas only one size was studied for arteriole flow. NPs were designed to be released from the upper inlet of the tube. The parameters used for these simulations are detailed in the Table 3.6 below.

Table 3.6: Flow and Particle Parameters used for Blood Flow Simulation and Particle Tracing.

Particle simulation parameters for both models					
Model	**Flow Rate**	**Viscosity**	**RBC Diameter**	**NP Diameter**	**NP Releasing**
Capillary	$6 \cdot 10^{-6} ml/min$	1.2 cP	$7\mu m$	180 nm & 250 nm	10 per ms
Arteriole	500 ml/min	4 cP	$7\mu m$	180 nm	100 per 50 ms

4

Results and Discussion

4.1 Literature Study

This literature study covered various aspects that could improve the VoC setup and NP measurements. Both PDL and poly-L-lysine (PLL) are commonly used coating materials for cell culture [44], but PDL was chosen for the experiments over PLL because PDL is resistant to degradation by cellular proteases [45]. It performs better if dried overnight and adds the benefit of being a non-animal material. VE-cadherin is one of the key proteins involved in the cell junction and formation of monolayer [26]. Therefore, it is frequently used to assess the function of EC monolayer during microvascular studies. For instance, Zheng's study utilized immunofluorescence staining of VE-cadherin to study the migration and permeability of human pulmonary microvascular endothelial cells (HPMECs).

4.2 VoC Optimization

4.2.1 Evaluation of Microfluidic Pump Setup for Long-Term Stability

Figure 4.1A and Figure 4.1C illustrate the microfluidic system, including the Falkon tube, connectors and 1-1.5 meter silicon tube with either the BEOnChip or the Ibitreat chip. After 24 hours of flow, the system showed no signs of leakage or breakage. However, the recirculated cell medium became cloudy and the characteristic pink color of the cell medium faded, as shown in 4.1B. Upon observation, the cause of this change in the cell medium was a breakdown inside the tubing. Figure 4.1D illustrates the part of silicon connected to the pump had become thinner and was damaged. This breakage was caused by mechanical stress under long-term flow and resulted in crushed silicon inner sections entering into the cell medium as small white flakes, resulting in the cloudy cell medium.

Therefore, it was deemed necessary to replace the silicon tubing at least every 24 hours to maintain system integrity and avoid the silicon flakes damaging the cells in the chip channel. Regular inspection and a stable fluidic environment are essential for VoC building up.

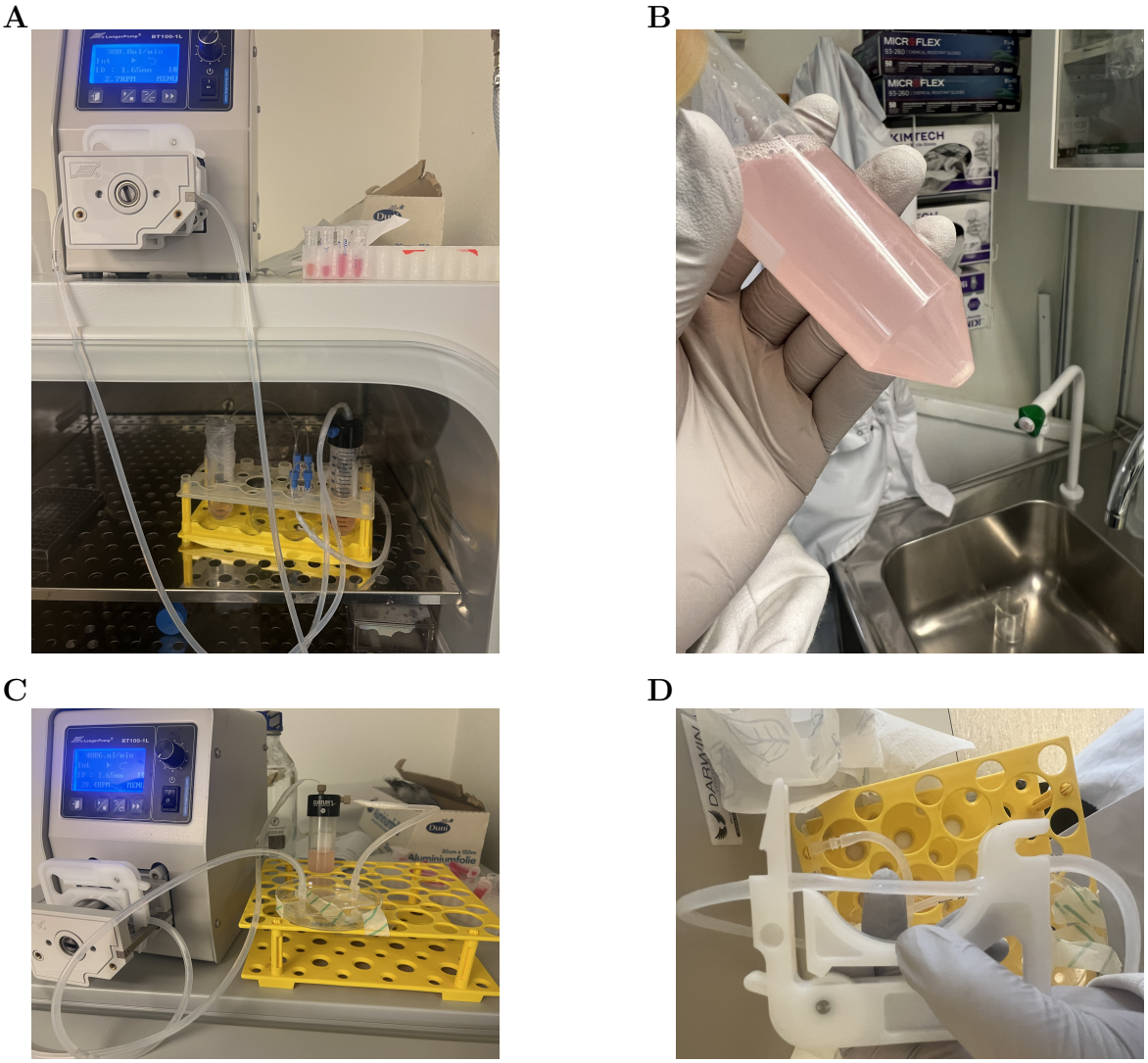

Figure 4.1: Photos of the optimized microfluidics set-up. (A) Optimized set-up with BEOnChip. (B) Cloudy cell medium was observed during the experiment. (C) Optimized set-up with Ibidi chip. (D) Thinned silicon tube was observed.

4.2.2 Setup using BEOnChip

Table 4.1 summarizes the attempts and results from VoC experiments utilizing two kinds of BEOnChips including different coating materials and flow speeds. As shown in 4.2A, ECs were randomly oriented and tightly connected. As shown in Figure 4.2C, all ECs besides those near the channel edge detached from the surface after 5 hours of flow at $300\mu l/min$, additionally, the entire COLI coating layer detached as well.

Table 4.1: Results of Flow Tests Using BEOnChips Under Different Setups

Flow Results Summary with BEOnChips					
Date	**Coating Material**	**Culture Time**	**Flow Rate (μl)**	**Flow Time**	**Results**
14/02	PDL	4h	400	4h	No cells left
19/02	PDL	4h	300	2h	No cells left
19/02	PDL*2	4h	300	2h	No cells left
21/02	PDL	20h	300	4h	No cells left
21/02	PDL*2	20h	300	4h	No cells left
29/02	PDL	22h	300	4h	No cells left
29/02	COL I	22h	300	4h	Some cells left but damaged by flow from another PDL channel
06/03	COL I	48h	300	4h	No cells left
08/03	COL I+PDL	18h	100 (1.5h) 200 (1h) 400 (1h) 600	4h	Some cells at 3 hours, no cells left at 5 hours
07/03	COL+I	18h	200 (1h) 400 (1h) 600	4h	No cells left
12/03	COL I+PDL	24h	100 (1h) 200 (1h) 400 (1h) 600	4h	No cells left
14/03	COL I+PDL	24h	150	24h	No cells left

To enhance the attachment of the cells, two types of coating materials were mixed. As seen in Figure 4.2B, the cells attached well on the surface after 2.5 hours of flow at $200\mu l/min$. This improvement could be due to the PDL enhancing the coating adherence. However, the adhesion was still insufficient as the cells did not align and began to detach when the flow rate increased. The conclusion was that the adhesion of the chip did not support a physiologically relevant fluidic system and new alternatives for the microfluidic chip had to be decided in order to allow the cells to maintain attached to the surface and be triggered to align at the expected shear stress level.

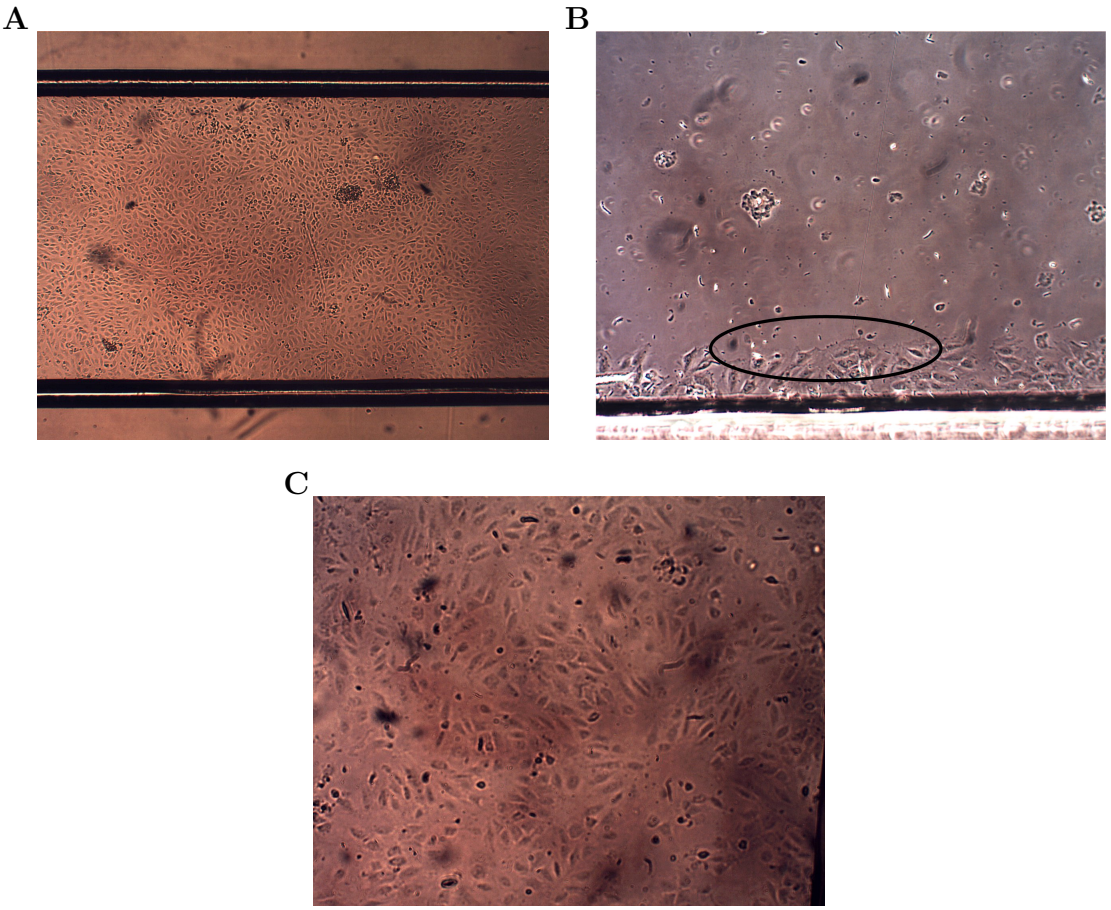

Figure 4.2: 4X phase contrast microscopy images of channels of BEOnChips. (A) BE-FLOW chip before flow. (B) BE-FLOW chip after 5h flow. (C) BE-FLOW chip using mixed coating material after 2.5 hours at flow rate $200\mu l/min$.

4.2.3 Setup using Ibidi Chips and Alignment Confirmation

Table 4.1 below summarizes the results from VoC experiments utilizing Ibitreat and IbGlass chip including the date, coating materials, cell culture time, flow set-up, and results.

Table 4.2: Results of Flow Tests Using Ibidi Chips Under Different Flow and Coating Setups.

Flow Results Summary with Ibidi chips						
Date	**Chip**	**Coating Material**	**Culture Time**	**Flow Rate (ml/min)**	**Flow Time**	**Results**
21/03	Ibitreat	COLI	20h	1(1h) 2(1h) 5(17h) 9(4h)	>24h	Align after 28h.
26/03	IbGlass	COLI	24h	1.2(1h) 2.4(1h) 7ml(24h)	>24h	Align after 24h.
09/04	Ibitreat	PDL	20h	1(1h) 2(1h) 5(17h) 9(4h)	>24h	Align after 24h, but some cells detached.
09/04	IbGlass	PDL	24h	1.2(1h) 2.4(1h) 7(24h)	>24h	Align after 24h.
16/04	Ibitreat	COLI	20h	1(0.5h) 2(1h) 5(1h) 9(22h)	>24h	Align after 24h, alive after 4 days.
06/05	Ibitreat	COLI	6h	2(0.5h) 5(1h) 9(>22h)	>24h	Aligned after 24h flow

The alignments of the ECs at all attempts could be observed after about 24 hours of continuous flow, as in Figures 4.3A and 4.3B. The MATLAB code was used for evaluating the angle of the orientation of cells along flow direction as Figures 4.3C and 4.3D shown. The angle distribution, ranging from -90 to 90 degrees, was plotted in histogram 4.3E. The blue bars represented the angle of ECs under static condition, while the red bars represented the angle distribution of ECs after 24 hours of flow.

Compared to the chips from BEOnChip and Ibidi, the chip material was the key factor that influenced the adhesion of the cell to the chip surface. The COC and COP of the BEOnChip could not provide an adhesive enough surface for either the cell or the coating material. In contrast, both polymer and glass surfaces of the Ibidi chip demonstrated superior adhesion properties.

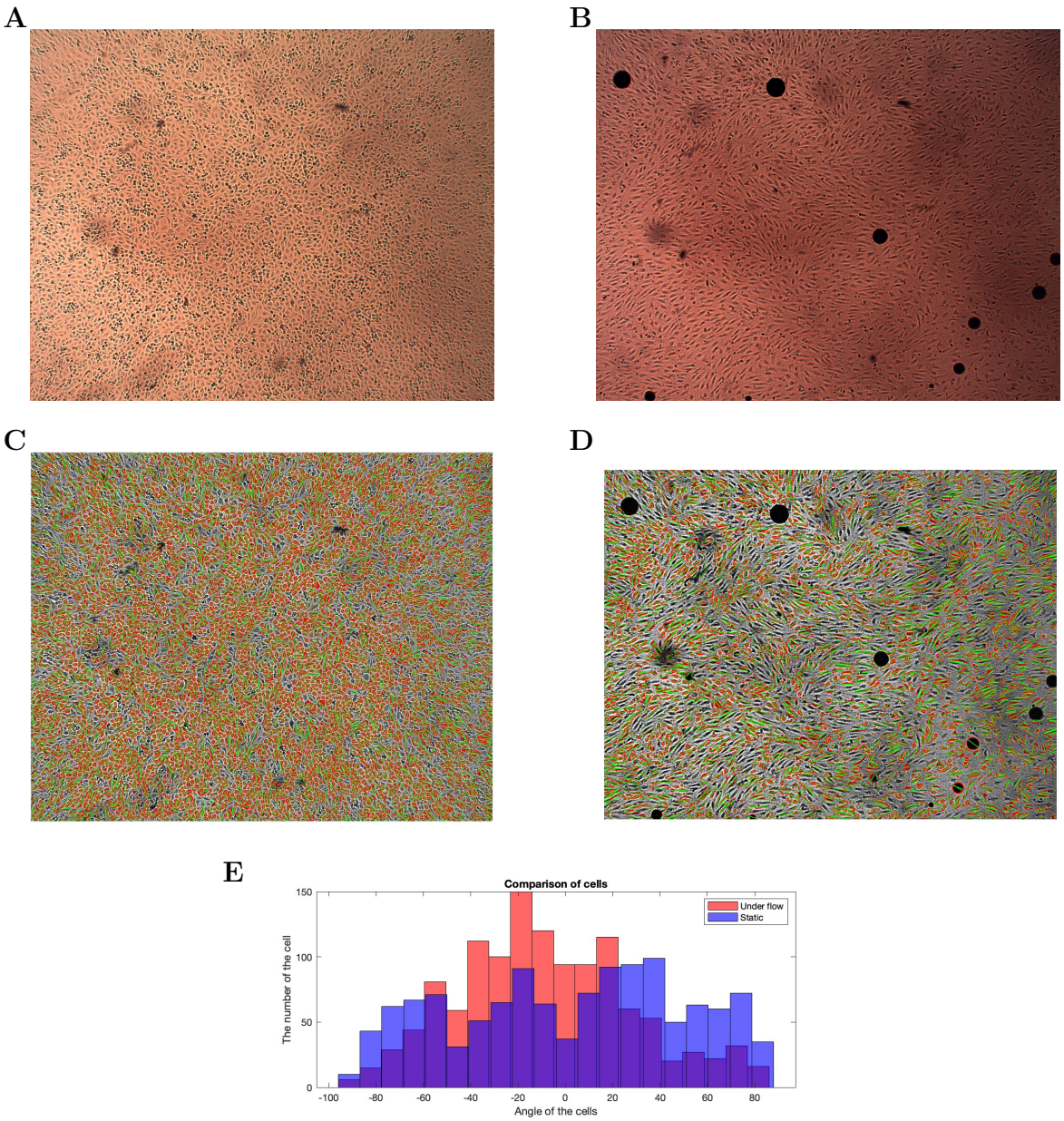

Figure 4.3: EC alignment condition inside the Ibitreat chip. (A) 4X phase contrast microscopy images of ECs inside Ibitreat channel coated with COLI before flow. (B) 4X phase contrast microscopy images of ECs inside Ibitreat channel coated with COLI after 24-hour flow. (C) Cell detection and direction calculation before flow. (D) Cell detection and direction calculation after flow. (E) Cell direction histogram of figures (C) and (D).

Two phenomena were observed during the experiments. As shown in Figure 4.4A, the ECs remained viable after 4 days of flow. However, the cells in the middle of the chip exhibited a swirled alignment to each other, indicating the flow became more turbulent rather than laminar. This was most probably caused by the wide size of the channel, as the fact that more turbulent flow occurs in larger vessels. Another observation was seen near the inlet of the Ibidi chip as illustrated in Figure 4.4B,

the majority of the ECs in this area detached from the surface, possibly caused by the higher pressure near the inlet area.

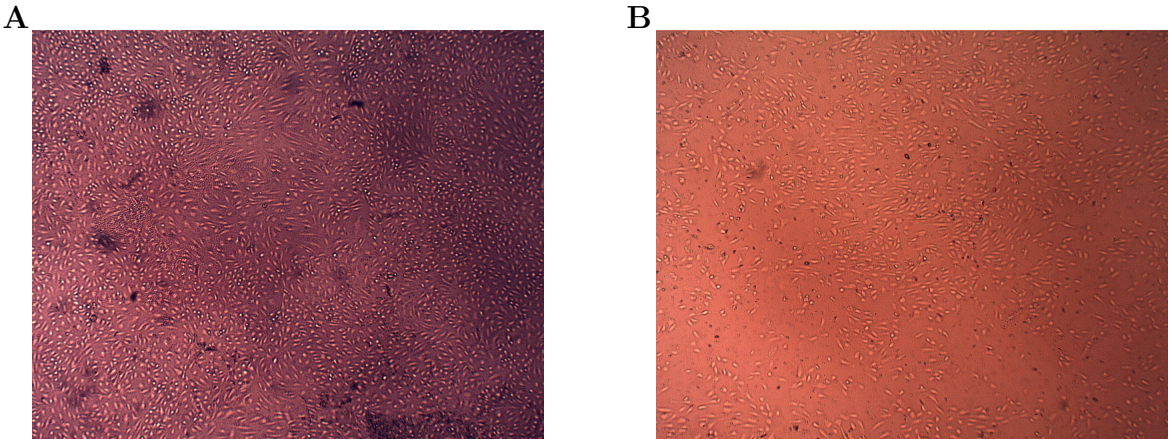

Figure 4.4: 4X phase contrast microscopy images of two special observations during the Ibidi chip fluidics experiment. (A) EC layer using Ibitreat chip coated with COLI before flow after 4-day flow. (B)ECs near the inlet of Ibitreat chip with PDL coating after 24-hour flow.

4.3 NP Extravasation Evaluation over the Endothelial Monolayer

4.3.1 Under Static Condition

The evaluation of NP extravasation was conducted with a confocal microscope to measure NP transportation through the EC monolayer after the confirmation of the EC alignment. The cells were tightly oriented initially as shown in Figure 4.5A, with clear visualization of the blue-stained nuclei and the cell membranes within 10 minutes after NP added to the channel. After 3 hours of incubation, the boundaries of the blue nuclei were not as clear, and junctions between cells widened in Figure 4.5B, indicating the cells lost viability. Compared to the microfluidic experiment results, where the cells exhibited good viability under 4 days of flow, the assumption was either the static condition reduced the viability or the NPs damaged the ECs.

Figure 4.5C illustrates a flipped view of the z-stacked image, the z-slices were arranged from top to bottom. The corresponding blue and green fluorescence signal intensity in each z-slice were calculated and then plotted in Figure 4.5D. The peak in the blue signal curve represented the center of the EC monolayer, while the intensity of the FITC fluorescence rapidly decreased near this layer. Given the thickness of ECs is approximately 10 μm, ± 5 μm around the layer with the blue peak value could be estimated as the section of the EC monolayer. These estimated inner cellular layers were illustrated in transparent red color in Figure 4.5E. Thus, depth 10

μm at the z-axis was estimated to be the upper membrane, while depth 20 μm at the z-axis was the lower membrane.

Looking closely at this upper membrane layer at 10 μm, the intensity of the fluorescence increased over time gradually, rising from an intensity value of 8.4 at 10 min (blue curve) to 12 at 2 hours (green curve) in Figure 4.5E. NPs appeared to accumulate on the EC wall by gravitational effects over time. The increase of the intensity further proved the result that the NPs stayed at the membrane surface and could not transport over the monolayer.

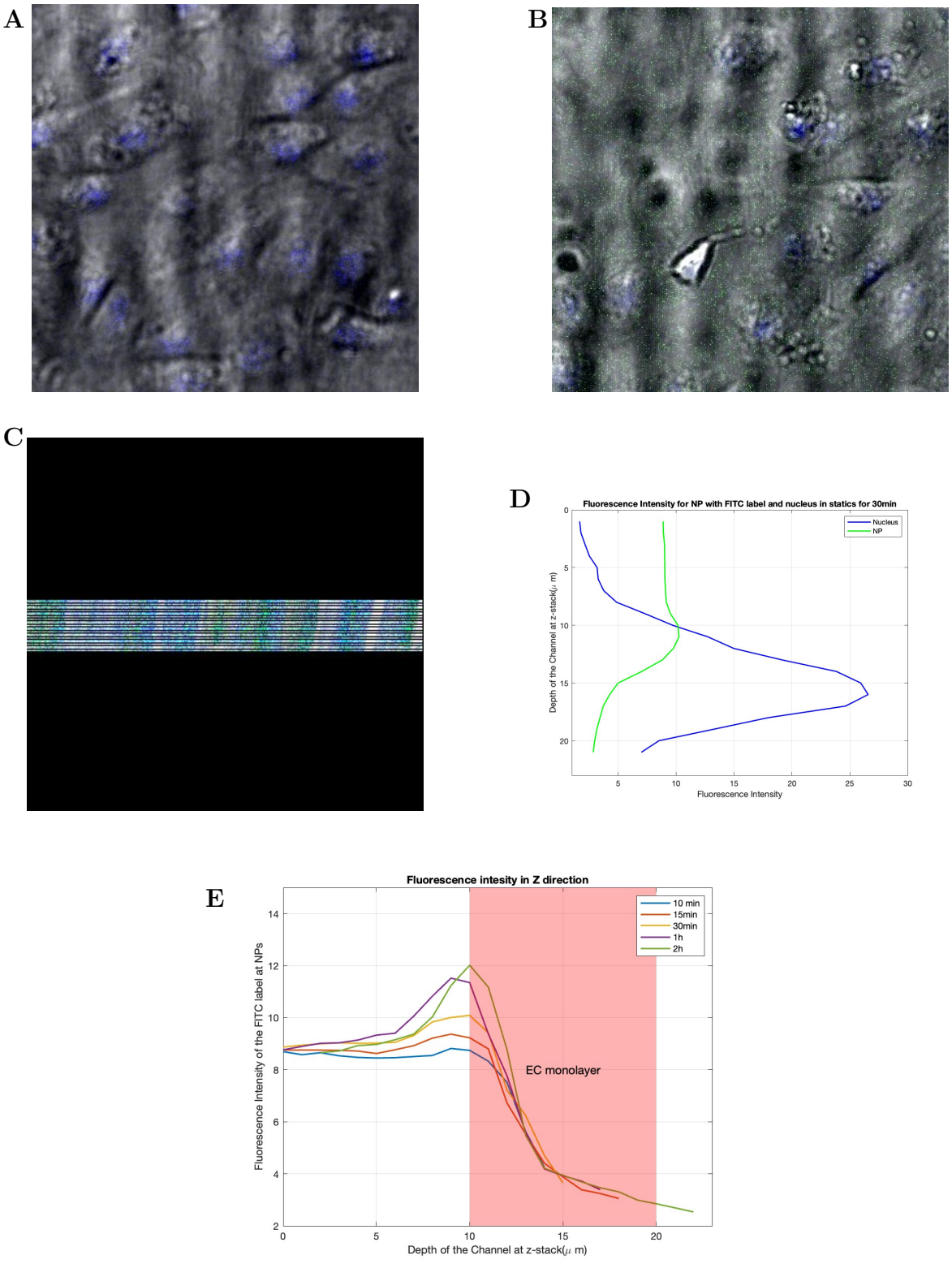

Figure 4.5: Images of NP transportation through EC layer under static condition. (A) Merged 20X confocal images of the monolayer at 10 min under static conditions. (B) Merged 20X confocal images of the monolayer after 3 hours in statics. (C) Flipped z-stack images. (D) The NP and nucleic fluorescence intensity plot at each z-stack. (E) The NP fluorescence intensity plot in different time points, the red area represents the inner cellular part.

In this experiment, the NPs were incubated and seeded into the channel with HUVEC cell medium under static condition. No evidence of NP extravasation over the endothelial monolayer was observed and the NPs remained on the membrane. The interaction between the NP and cell membrane has not been confirmed, the NP aggregation near the surface might have contributed to the non-extravasation result. Moreover, the cells lost viability quickly under static conditions, which could have impacted the NP transportation as well.

4.3.2 Under flow Condition

The same NP measurement was performed but under flow conditions with 10% FBS added to the cell medium. The ECs were well aligned in Figure 4.6A. Figure 4.6C illustrates a flipped view of Figure 4.6A, the z-slices were arranged from top to bottom. To gather more information, more slices of the sample were captured and a bigger step size was used compared to the under static condition. The corresponding blue and green fluorescence signal intensity of each z-slice were evaluated and then plotted in Figure 4.6D. The location of the monolayer was determined also based on the high blue florescent peak in the plot.

These evaluated inner cellular layers were marked with red color in Figure 4.6B, and the upper membrane was estimated to be at depth 25 μm at the z-axis. The intensity of the FITC fluorescence decreased with time, comparing the blue curve at 10 minutes and the yellow at 2 hours. Since the NPs in the cell medium suspension were recirculated within the microfluidic system, the decreased intensity could be caused by the NPs attached to the silicon tube wall. Another reason could be the FITC label got photo-bleached during the long time measurement[46]. The exposure to light could not be completely avoided since utilizing a transparent silicon tube in the fluidic system.

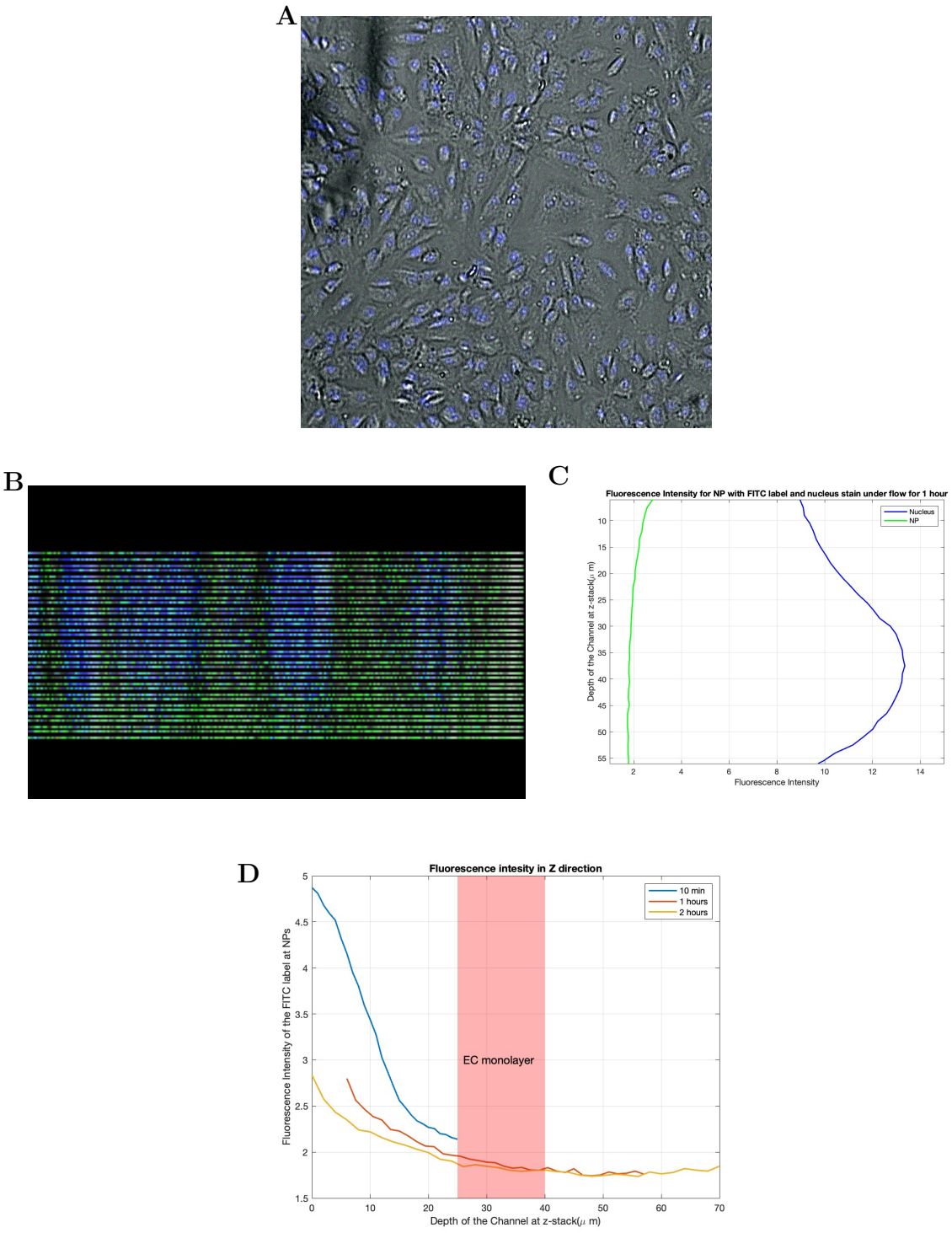

Figure 4.6: Images of NP transportation through EC layer under flow condition. (A) Merged confocal images of the monolayer at 1 hour underflow. B Flipped image from the z-stack images at 1 hour. (C) The NP and nucleic fluorescence intensity plot at each z-stack layer. (D) The NP fluorescence intensity plot in different time points, the red area represents the inner cellular part.

Though a weak signal of green fluorescence could still be detected inside the cell

layer and COLI coating layer under the ECs, it did not prove that the NP had transported from upside down through the monolayer. COLI is a protein with a complex structure, some cross-links and amino acid residues in collagen are capable of autofluorescence [47], which led to a weak signal of green at the depth lower than 35 μm in the z-axis in Figure 4.6B.

Experiments under both conditions suggested that the transportation mechanism through the vessel wall for this PLGA NP was likely endocytosis, which suggests stimuli application to the cells might be required to activate the endocytosis pathway. The lack of NPs extravasation could be caused by the large diameter of the NPs and the tight junctions between ECs. Moreover, the FBS was added during the experiment, the protein inside the serum could lead to the PC effect. The PC effect and the interaction between the NPs and the EC membranes could further increase the size and decrease the mobility of the NPs. In comparison to the previous work of this project, where the ECs had not formed a monolayer and therefore had much larger junctions between the ECs, the NP could be captured under that non-aligned cell layer.

Another important consideration is the different structures and functions between healthy endothelium and diseased endothelium. In many diseases, such as primary tumors could send inflammatory stimulation, leading to endothelium dysfunction at both cellular and molecular levels[48]. This pro-inflammatory response causes changes in vascular, including discontinuation of the monolayer, degradation of the junction proteins, and increased permeability through the endothelial[49]. In Kwak's study, the NP could pass through the blood vessel channel to the tumor channel. however, the blood flow shear stress was set at 0.1 dyn/cm^2 [42]. This shear stress level is 100 times lower than the level required for the ECs to align. Therefore, the non-aligned EC layer could be considered a representative of endothelium inside the diseased target tissue and used as a control group compared to the aligned monolayer. In another study on tumor and ECs interactions using OoC, the majority of the NP that transported through ECs to tumor cells had a diameter of 40 nm before stimulation was added into the model [50]. After transient receptor potential vanilloid 4 stimulation was introduced into the microfluidic channel, the adherens junctions between ECs were disrupted, accelerating NPs extravasation of various sizes, including 20 nm, 50nm, and 200nm.

4.4 Simulation of Flow and NP Attachment

4.4.1 Microfluidic Chip Simulation

Figure 4.7A illustrates the velocity field inside the BEOnChip channel, the white arrows represent the direction field of the flow. Figure 4.7B shows the shear stress distribution inside the BEOnChip channel, with a slice of the shear stress field at the yz plane to display the vertical status of the shear stress. Figure 4.7C illustrates the

velocity field inside the Ibitreat chip channel, the red arrows represent the direction field of the flow. Figure 4.7D shows the shear stress distribution inside the Ibitreat channel, with a yz-plane slice to display the vertical status of the shear stress.

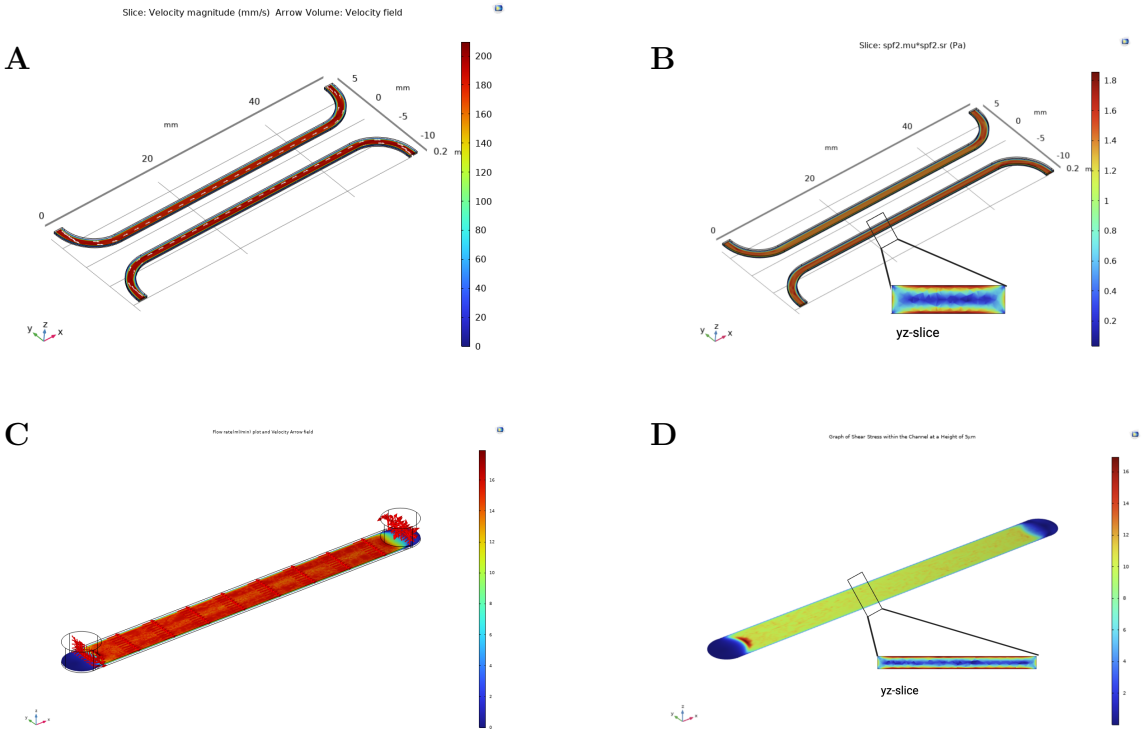

Figure 4.7: Plots of flow simulation results of both BEOnChips and Ibitreat chip. (A) Velocity field flow rate plot of BEOnChip simulation. (B) Shear stress plot of BEOnChip simulation, and yz-slice plot of shear stress in the channel. (B)Velocity field flow rate plot of Ibitreat chip simulation. (D) Shear stress plot of Ibitreat simulation, and yz-slice plot of shear stress in the channel.

The average shear stress for both the BEOnChip channel surface and the Ibitreat channel surface is around $10 dyn/cm^2$ as shown in Figure 4.7D. However, the sheer stress value close to the Ibitreat chip inlet is much higher than $10 dyn/cm^2$, as the red area shown in Figure 4.7D. This result matched the VoC experiment utilizing Ibitreat in Figure 4.4B, where the ECs detached from the surface due to the higher shear stress.

4.4.2 Blood Flow Simulation with RBCs and NPs

Both capillary flow and arteriole flow models were built up and simulated with RBCs and NPs. Figure 4.8A and Figure 4.8D demonstrate the capillary flow and arteriole flow along with RBCs and NPs. Figure 4.8B and Figure 4.8E demonstrate the NP attached to the vessel walls for both models. The attachment result of both models is listed in Table 4.3.

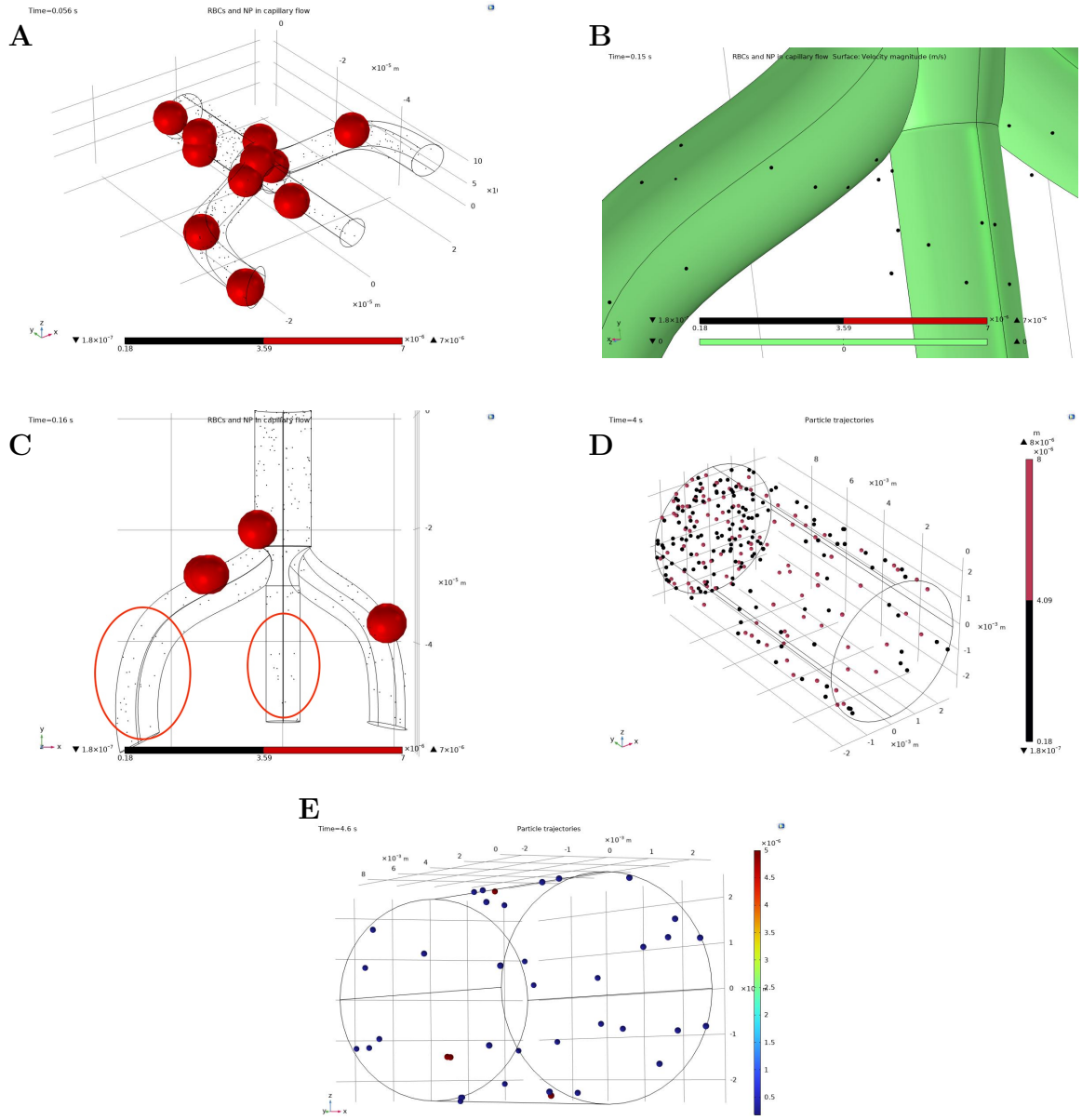

Figure 4.8: Plot of blood flow simulation and NP adhering result. (A) Red blood cells and nanoparticles traveling within the capillary flow model. (B) The surface of the capillary wall was modified to green to visualize particles adhering to the vessel wall. (C) Attachment of nanoparticles at different capillary shapes, highlighted in the circled areas. The left circle shows a curved capillary, while the middle depicts a straight capillary. (D) Red blood cells and nanoparticles traveling within the arteriole flow model. (E) Attachment of nanoparticles at arteriole wall.

Table 4.3: Table of NP Attachment Results.

Simulation Results of the Attached NP ratio on the Vessel Wall				
Model	NP diameter	Released NP	Stuck NP	Ratio
Capillary	250nm	1000	221	22.1 %
	180nm	1000	287	28.7 %
Arteriole	180nm	8910	34	0.4%

The high flow rate in the arteriole led to significantly less NP attached to the wall compared to the capillary flow model, indicating the low potential for NP uptake. The NPs of 180nm exhibit a slightly higher ratio of NP attachment compared to the 250nm NPs, which was not as initially expected. In another simulation study that established an NP-RBC interaction model suggested that the interaction between smaller NPs and RBCs had limited adhesion of these NPs to the vessel wall [51]. Thus, the bigger NPs were expected to acquire a higher uptake ratio.

The shape of the vessel could also affect the attachment ratio of the NP, as Figure 4.8C shows. More NPs were attached to the surface in the left circled area, indicating that the NPs had a higher uptake ratio in the curved capillaries than the straight capillaries. In general, the NPs showed a greater potential for uptake in a capillary network with curved tubular structure than larger arterioles characterized by more linear tubular structure.

However, the current model's results were limited because it only included laminar flow dynamics and particle tracing modules. This limitation means the results were not fully comprehensive, for example, the turbulent flow inside a big vessel could lead to more attachment of the NP on the surface. To achieve a more complete simulation study of NP behavior in vascular systems, future models should incorporate additional factors such as cellular and NP interactions, and physical representation of RBC.

5
Conclusion

The study demonstrated that both Ibitreat and IbGlass successfully supported the optimized microfluidic setup, although the silicon tube required regular inspection and some random turbulence was observed in the wide channel. BEonChips could not be utilized in our VoC setup and are therefore not recommended for future EC monolayer constructions. Under both static and flow conditions, NPs showed no evidence of extravasation over the EC monolayer, indicating the transportation of the 190nm PLGA NP is most likely endocytosis or requires larger junction.
Simulations of chip flow closely matched wet-lab observations, proving the simulations are a valuable tool for biological studies. The blood flow simulation results also indicated that NPs were more likely to attach to the capillary walls compared to larger vessels with higher flow rates. Despite the success of building up the VoC and blood flow models, the results are preliminary and more studies are needed to make a definitive conclusion.

5.1 Future initiative

To complete the study, future initiatives are pursued in both wet-lab experimentation and computational modeling.

In the wet lab, efforts could focus on repeating NP uptake studies to validate results and ensure reproducibility. Additionally, exploring methods to add biological or chemical stimuli to the EC monolayer might trigger the channel for the NPs uptake through the monolayer. Improving the staining techniques and avoiding autofluorescence of the coating material could increase the visualization and analysis of NPs under the confocal microscope. Furthermore, another chip from Ibidi with a narrow channel of 2mm is recommended for future VoC use to avoid artifacts of random turbulent flow inside the wide chip.
Another approach that could be added to the project is using EC under static conditions or under the flow with a much low shear stress to represent the dysfunctional capillary wall. By comparing the transmit ratio at the healthy state and disordered state, a more comprehensive understanding of NP delivery to the target tissues could be potentially achieved.

On the computational side, initiatives should involve developing computational models to simulate turbulent flow conditions within microfluidic systems, providing more

realistic representations of fluid dynamics. Enhancing simulations by including physically representative models of RBCs would allow for more accurate predictions of NP-RBC interactions and their effects on vascular dynamics since RBCs have a special shape. These future initiatives are intended to advance our understanding of NP behavior in vascular systems and facilitate the design of nanomedicine in a more effective and mimic-human-biology approach.

Bibliography

[1] K. Riehemann, S. Schneider, T. Luger, B. Godin, M. Ferrari, and F. Harald, "Nanomedicine-challenge and perspectives," *Angewandte Chemie (International ed. in English)*, vol. 48, pp. 872–97, Feb. 2009. DOI: 10.1002/anie.200802585.

[2] N. Pardi, M. Hogan, F. Porter, and D. Weissman, "Mrna vaccines — a new era in vaccinology," *Nature Reviews Drug Discovery*, vol. 17, Jan. 2018. DOI: 10.1038/nrd.2017.243.

[3] R. Thapa and J. Kim, "Nanomedicine-based commercial formulations: Current developments and future prospects," *Journal of Pharmaceutical Investigation*, vol. 53, Dec. 2022. DOI: 10.1007/s40005-022-00607-6.

[4] C. Oerlemans, W. Bult, M. Bos, G. Storm, J. Nijsen, and W. Hennink, "Polymeric micelles in anticancer therapy: Targeting, imaging and triggered release," *Pharmaceutical research*, vol. 27, pp. 2569–89, Dec. 2010. DOI: 10.1007/s11095-010-0233-4.

[5] D. Sun, S. Zhou, and W. Gao, "What went wrong with anticancer nanomedicine design and how to make it right," *ACS Nano*, vol. 14, no. 10, pp. 12 281–12 290, 2020, PMID: 33021091. DOI: 10.1021/acsnano.9b09713. eprint: https://doi.org/10.1021/acsnano.9b09713. [Online]. Available: https://doi.org/10.1021/acsnano.9b09713.

[6] X. Shan, X. Gong, J. Li, J. Wen, Y. Li, and Z. Zhang, "Current approaches of nanomedicines in the market and various stage of clinical translation," *Acta Pharmaceutica Sinica B*, vol. 12, no. 7, pp. 3028–3048, 2022, ISSN: 2211-3835. DOI: https://doi.org/10.1016/j.apsb.2022.02.025. [Online]. Available: https://www.sciencedirect.com/science/article/pii/S2211383522000818.

[7] R. Augustine, A. Hasan, R. Primavera, R. J. Wilson, A. S. Thakor, and B. D. Kevadiya, "Cellular uptake and retention of nanoparticles: Insights on particle properties and interaction with cellular components," *Materials Today Communications*, vol. 25, p. 101 692, 2020, ISSN: 2352-4928. DOI: https://doi.org/10.1016/j.mtcomm.2020.101692. [Online]. Available: https://www.sciencedirect.com/science/article/pii/S2352492820327033.

[8] C. Dong, A. Ma, and L. Shang, "Animal models used in the research of nanoparticles for cardiovascular diseases," *Journal of Nanoparticle Research*, vol. 23, Aug. 2021. DOI: 10.1007/s11051-021-05289-z.

[9] I. Khan, K. Saeed, and I. Khan, "Nanoparticles: Properties, applications and toxicities," *Arabian Journal of Chemistry*, vol. 12, no. 7, pp. 908–931, 2019, ISSN: 1878-5352. DOI: https://doi.org/10.1016/j.arabjc.2017.05.011.

[Online]. Available: https://www.sciencedirect.com/science/article/pii/S1878535217300990.

[10] R. Herrero-Vanrell, A. Rincón, M. Alonso, V. Reboto, I. Molina-Martinez, and J. Rodríguez-Cabello, "Self-assembled particles of an elastin-like polymer as vehicles for controlled drug release," *Journal of Controlled Release*, vol. 102, no. 1, pp. 113–122, 2005, ISSN: 0168-3659. DOI: https://doi.org/10.1016/j.jconrel.2004.10.001. [Online]. Available: https://www.sciencedirect.com/science/article/pii/S0168365904004730.

[11] M. Nikzamir, A. Akbarzadeh, and Y. Panahi, "An overview on nanoparticles used in biomedicine and their cytotoxicity," *Journal of Drug Delivery Science and Technology*, vol. 61, p. 102 316, 2021, ISSN: 1773-2247. DOI: https://doi.org/10.1016/j.jddst.2020.102316. [Online]. Available: https://www.sciencedirect.com/science/article/pii/S1773224720316051.

[12] S. Wilhelm, A. Tavares, Q. Dai, *et al.*, "Analysis of nanoparticle delivery to tumours," *Nature Reviews Materials*, vol. 1, p. 16 014, Apr. 2016. DOI: 10.1038/natrevmats.2016.14.

[13] A. K. Mohammad and J. Reineke, "Quantitative detection of plga nanoparticle degradation in tissues following intravenous administration," *Molecular pharmaceutics*, vol. 10, Mar. 2013. DOI: 10.1021/mp300559v.

[14] H. Li, Y. Wang, Q. Tang, *et al.*, "The protein corona and its effects on nanoparticle-based drug delivery systems," *Acta Biomaterialia*, vol. 129, May 2021. DOI: 10.1016/j.actbio.2021.05.019.

[15] I. Alberg, S. Kramer, M. Gangluff, *et al.*, "Polymeric nanoparticles with neglectable protein corona," *Small*, vol. 16, p. 1 907 574, Apr. 2020. DOI: 10.1002/smll.201907574.

[16] V. Muzykantov and S. Muro, "Targeting delivery of drugs in the vascular system," *International journal of transport phenomena*, vol. 12, pp. 41–49, Jan. 2011.

[17] R. Freitas, "Nanomedicine, volume i: Basic capabilities," in Jan. 1999, p. 509.

[18] H. Minasyan, "Bactericidal capacity of erythrocytes in human cardiovascular system," *International Clinical Pathology Journal*, vol. 2, Jul. 2016. DOI: 10.15406/icpjl.2016.02.00052.

[19] M. Félétou, "The endothelium, part i: Multiple functions of the endothelial cells – focus on endothelium-derived vasoactive mediators," *Colloquium Series on Integrated Systems Physiology: From Molecule to Function*, vol. 3, pp. 1–306, Jun. 2011. DOI: 10.4199/C00031ED1V01Y201105ISP019.

[20] W. Aird, "Aird, w. c. phenotypic heterogeneity of the endothelium: I. structure, function and mechanisms. circ. res. 100, 158-173," *Circulation research*, vol. 100, pp. 158–73, Mar. 2007. DOI: 10.1161/01.RES.0000255691.76142.4a.

[21] C. Potter, S. Schobesberger, M. Lundberg, P. Weinberg, J. Mitchell, and J. Gorelik, "Shape and compliance of endothelial cells after shear stress in vitro or from different aortic regions: Scanning ion conductance microscopy study," *PloS one*, vol. 7, e31228, Feb. 2012. DOI: 10.1371/journal.pone.0031228.

[22] W. Adams, Y. Zhang, J. Cloutier, *et al.*, "Functional vascular endothelium derived from human induced pluripotent stem cells," *Stem cell reports*, vol. 1, pp. 105–13, Aug. 2013. DOI: 10.1016/j.stemcr.2013.06.007.

[23] E. Vandenbroucke, D. Mehta, R. Minshall, and A. Malik, "Regulation of endothelial junctional permeability," *Annals of the New York Academy of Sciences*, vol. 1123, pp. 134–45, Apr. 2008. DOI: 10.1196/annals.1420.016.

[24] A. Misra, *Challenges in Delivery of Therapeutic Genomics and Proteomics*. Jan. 2011. DOI: 10.1016/C2010-0-65663-X.

[25] D. Rubenstein, W. Yin, and M. Frame, "In vitro biofluid mechanics," in Jan. 2022, pp. 573–589, ISBN: 9780128180341. DOI: 10.1016/B978-0-12-818034-1.00016-5.

[26] N. Duong and D. Vestweber, "Mechanisms ensuring endothelial junction integrity beyond ve-cadherin," *Frontiers in Physiology*, vol. 11, p. 519, May 2020. DOI: 10.3389/fphys.2020.00519.

[27] M. Giannotta, M. Trani, and E. Dejana, "Ve-cadherin and endothelial adherens junctions: Active guardians of vascular integrity," *Developmental cell*, vol. 26, pp. 441–54, Sep. 2013. DOI: 10.1016/j.devcel.2013.08.020.

[28] K. Katoh, Y. Kano, and S. Ookawara, "Role of stress fibers and focal adhesions as a mediator for mechano-signal transduction in endothelial cells in situ," *Vascular health and risk management*, vol. 4, pp. 1273–82, Feb. 2008.

[29] N. Munshi and S. Jagannath, "Plasma cell neoplasms," in Jan. 2018, 1381–1418.e1, ISBN: 9780323357623. DOI: 10.1016/B978-0-323-35762-3.00086-X.

[30] T. Secomb, "Hemodynamics," *Comprehensive Physiology*, vol. 6, pp. 975–1003, Mar. 2016. DOI: 10.1002/cphy.c150038.

[31] S. Lynch, N. Nama, and C. Figueroa, "Efects of non-newtonian viscosity on arterial and venous fow and transport," *Scientific Reports*, vol. 12, p. 20 568, Nov. 2022. DOI: 10.1038/s41598-022-19867-1.

[32] E. Nader, S. Skinner, M. Romana, *et al.*, "Blood rheology: Key parameters, impact on blood flow, role in sickle cell disease and effects of exercise," *Frontiers in Physiology*, vol. 10, Oct. 2019. DOI: 10.3389/fphys.2019.01329.

[33] M. Ameenuddin, M. Anand, and M. Massoudi, "Effects of shear-dependent viscosity and hematocrit on blood flow," *Applied Mathematics and Computation*, vol. 356, pp. 299–311, Sep. 2019. DOI: 10.1016/j.amc.2019.03.028.

[34] M. Ascolese, A. Farina, and A. Fasano, "The fåhræus-lindqvist effect in small blood vessels: How does it help the heart?" *Journal of Biological Physics*, vol. 45, Dec. 2019. DOI: 10.1007/s10867-019-09534-4.

[35] B. Rehm, A. Haghshenas, A. Paknejad, and J. Schubert, "Situational problems in mpd," in Dec. 2013, pp. 39–80, ISBN: 9781933762241. DOI: 10.1016/B978-1-933762-24-1.50008-5.

[36] R. Reneman, T. Arts, and A. Hoeks, "Wall shear stress – an important determinant of endothelial cell function and structure – in the arterial system in vivo," *Journal of vascular research*, vol. 43, pp. 251–69, Feb. 2006. DOI: 10.1159/000091648.

[37] S. Chatterjee, "Endothelial mechanotransduction, redox signaling and the regulation of vascular inflammatory pathways," *Frontiers in Physiology*, vol. 9, Apr. 2018. DOI: 10.3389/fphys.2018.00524.

[38] S. Wolfe, "Vessel-on-a-chip models for studying microvascular physiology, transport, and function in vitro," *AJP Cell Physiology*, vol. 320, Nov. 2020. DOI: 10.1152/ajpcell.00355.2020.

[39] S. Kang, S. Park, and D. Huh, "Organ-on-a-chip technology for nanoparticle research," *Nano Convergence*, vol. 8, Dec. 2021. DOI: 10.1186/s40580-021-00270-x.

[40] X. Chen, Y. Zhang, X. Zhang, and C. Liu, "Organ-on-a-chip platforms for accelerating the evaluation of nanomedicine," *Bioactive Materials*, vol. 6, pp. 1012–1027, Apr. 2021. DOI: 10.1016/j.bioactmat.2020.09.022.

[41] K. Namdee, A. Thompson, P. Charoenphol, and L. Eniola-Adefeso, "Margination propensity of vascular-targeted spheres from blood flow in a microfluidic model of human microvessels," *Langmuir : the ACS journal of surfaces and colloids*, vol. 29, Jan. 2013. DOI: 10.1021/la304746p.

[42] B. Kwak, A. Ozcelikkale, C. Shin, K. Park, and B. Han, "Simulation of complex transport of nanoparticles around a tumor using tumor-microenvironment-on-chip," *Journal of controlled release : official journal of the Controlled Release Society*, vol. 194, Sep. 2014. DOI: 10.1016/j.jconrel.2014.08.027.

[43] COMSOL, *Comsol multiphysics user guide*, Version 6.1, COMSOL AB, 2023. [Online]. Available: https://doc.comsol.com/6.1/doc/com.comsol.help.mfl/MicrofluidicsModuleUsersGuide.pdf.

[44] D. Mazia, G. Schatten, and W. Sale, "Adhesion of cells to surfaces coated with polylysine. applications to electron microscopy," *The Journal of cell biology*, vol. 66, pp. 198–200, Aug. 1975. DOI: 10.1083/jcb.66.1.198.

[45] Biomat, *Poly-d or l-lysine coated surfaces*, Accessed: 2024-08-07, 2024. [Online]. Available: https://www.biomat.it/surfaces/poly-d-or-l-lysine-coated-surfaces/.

[46] J. Mahmoudian, R. Hadavi, M. Jeddi-Tehrani, *et al.*, "Comparison of the photobleaching and photostability traits of alexa fluor 568- and fluorescein isothiocyanate- conjugated antibody," *Yakhteh*, vol. 13, Apr. 2011.

[47] Ł. Saletnik and R. Wesołowski, "Fluorescent spectroscopy of collagen as a diagnostic tool in medicine," *Journal of Medical Science*, e584, Jan. 2022. DOI: 10.20883/medical.e584.

[48] T. Hsu, H.-H. Nguyen-Tran, and M. Trojanowska, "Active roles of dysfunctional vascular endothelium in fibrosis and cancer," *Journal of Biomedical Science*, vol. 26, Dec. 2019. DOI: 10.1186/s12929-019-0580-3.

[49] A. Amedei and L. Morbidelli, "Circulating metabolites originating from gut microbiota control endothelial cell function," *Molecules*, vol. 24, p. 3992, Nov. 2019. DOI: 10.3390/molecules24213992.

[50] M. Vu, P. Rajasekhar, D. Poole, *et al.*, "Rapid assessment of nanoparticle extravasation in a microfluidic tumor model," vol. 2, pp. 1844–1856, Apr. 2019. DOI: 10.1021/acsanm.8b02056.

[51] T.-R. Lee, M. Choi, A. Kopacz, S.-H. Yun, W. Liu, and P. Decuzzi, "On the near-wall accumulation of injectable particles in the microcirculation: Smaller is not better," *Scientific reports*, vol. 3, p. 2079, Jun. 2013. DOI: 10.1038/srep02079.

A

Appendix A

Equations involved in the simulations are based on the user's guide provided by COMSOL.
The Navier Stokes equations for laminar flow simulation in Stationary Study,

$\rho(u \cdot \bigtriangledown)u = \bigtriangledown \cdot (-p \cdot I + \mu(\bigtriangledown v + (\bigtriangledown v)^T)) + F$
$\rho \bigtriangledown \cdot v = 0$

The Navier Stokes equations for laminar flow simulation in Time-dependent Study,

$\rho\frac{\partial v}{\partial t} + \rho(v \cdot \nabla)v = \nabla \cdot \left(-pI + \mu(\nabla v + (\nabla v)^T)\right) + F$
$\rho\nabla \cdot v = 0$

Equation of the no-slip wall boundary condition:

$v = 0$

Where ρ is the density (SI unit: kg/m^3kg/m3), u is the velocity vector (SI unit: m/s), p is pressure (SI unit: Pa), F is the volume force vector (SI unit: N/m^3), and T is the absolute temperature (SI unit: K).

The Newtonian formulation is the default for the particle tracing module:

$\frac{d}{dt}(m_p\frac{q}{dt}) = 0$

where q (SI unit: m) is the particle position, m_p (SI unit: kg) is the particle mass.

The motion of particles in a flow is governed by Newton's second law, which states that the force on an object is equal to the time derivative of the object's linear momentum in an inertial reference frame as follows equations,

$\frac{d}{dt}(m_p v) = F_{tot}$
$F_{tot} = F_D + F_B$
$v = \frac{q}{dt}$

and F_{tot} (SI unit: N) is the total force on the particles which consists of drag force from the laminar flow F_D and Brownian force F_B.

The drag force formulation from the flow field is,

$$F_D = \frac{18\mu}{\rho_p {d_p}^2} m_p(u - v) = 0$$

In the equations above, v is the velocity of the particle (SI unit: m/s), u is the fluid velocity (SI unit: m/s) at the particle's position, ρ_p is the particle density (SI unit: $kg/m3$), and d_p is the particle diameter (SI unit: m).

The Brownian force equation is,

$$F_b = \zeta \sqrt{\frac{12\pi k_B \mu T r_p}{\Delta t}}$$

where Δt (SI unit: s) represents the time step taken by the solver, r_p (SI unit: m) is the particle radius, T(SI unit: K) is the absolute fluid temperature, μ(SI unit: $Pa \cdot s$) is the fluid dynamic viscosity, $k_B = 1.380649 \cdot 10^{-23} J/K$is the Boltzmann constant, and ζ(dimensionless) is a normally distributed random number with a mean of zero and unit standard deviation.

DEPARTMENT OF SOME SUBJECT OR TECHNOLOGY
CHALMERS UNIVERSITY OF TECHNOLOGY
Gothenburg, Sweden
www.chalmers.se

CHALMERS
UNIVERSITY OF TECHNOLOGY